

Impact of hydrogen addition, up to 20 % (mol/mol), on the thermodynamic (p , ρ , T) properties of a reference high-calorific natural gas mixture with significant ethane and propane content

Daniel Lozano-Martín¹, Heinrich Kipphardt², Peyman Khanipour², Dirk Tuma², Alfonso Horrillo^{3,4}, César Chamorro^{4,*}

¹ GETEF, Departamento de Física Aplicada, Facultad de Ciencias, Universidad de Valladolid, Paseo de Belén, 7, E-47011 Valladolid, Spain.

² BAM Bundesanstalt für Materialforschung und -prüfung, D-12200 Berlin, Germany.

³ CIDAUT Fundación, Plaza Vicente Aleixandre Campos, 2, E-47151, Boecillo-Valladolid, Spain

⁴ MYER, Departamento de Ingeniería Energética y Fluidomecánica, Escuela de Ingenierías Industriales, Universidad de Valladolid, Paseo del Cauce, 59, E-47011 Valladolid, Spain.

Abstract

Injecting hydrogen into the natural gas grid supports gradual decarbonization. To check the accuracy of equations of state for hydrogen-enriched natural gas mixtures, precise density data from well-characterized reference mixtures are essential. In a prior study, we provided experimental measurements for a natural gas constituted mainly of methane and for two derived hydrogen-enriched mixtures. In the present study, being the second and final part of our investigation, density measurements for a high-calorific natural gas with significant ethane and propane content, along with two hydrogen-enriched variants (10 and 20 mol-% hydrogen) are provided. The mixtures are gravimetrically prepared following ISO 6142-1. Density measurements, conducted with a single-sinker densimeter at temperatures from 260 to 350 K and pressures up to 20 MPa, are compared with three equations of state: AGA8-DC92, GERG-2008, and an improved GERG-2008. Results indicate that all models perform better for methane-dominant mixtures than for those containing heavier hydrocarbons.

Keywords: hydrogen-enriched natural gas; gravimetric preparation; single-sinker densimeter; high-pressure density; isothermal compressibility; reference equations of state

* Corresponding author e-mail: cesar.chamorro@uva.es.

List of Abbreviations

Nomenclature

k	Coverage factor
m	Mass, kg
M	Molar mass, kg/mol
N	Number of components of a mixture
p	Pressure, MPa
T	Temperature, K
u	Standard uncertainty
U	Expanded uncertainty
V	Volume, m ³
W	Balance reading, kg
W_s	Wobbe index
x	Molar fraction

Abbreviations

<i>AARD</i>	Average absolute value of relative deviation
AGA	American Gas Association
AGA8-DC92	AGA8-DC92 equation of state for mixtures
BAM	Federal Institute for Materials Research and Testing
<i>BiasRD</i>	Average relative deviation
GERG	Groupe Européen de Recherches Gazières
GERG-2008	GERG-2008 equation of state for mixtures
EoS	Equation of State
GC	Gas chromatography
GUM	Guide to the Expression of Uncertainty in Measurement
H2NG	Hydrogen-enriched natural gas
HHV	Higher heating value
LNG	Liquefied natural gas
<i>MaxRD</i>	Maximum relative deviation
NG	Natural gas
<i>RMSRD</i>	Root mean square relative deviation
UVa	University of Valladolid
VLE	Vapor-liquid equilibria

Greek symbols

α	Calibration factor
ε_ρ	Apparatus-specific constant
ϕ_0	Coupling factor
κ_T	Isothermal compressibility, Pa ⁻¹
ρ	Density, kg·m ⁻³
ρ_0	Reducing density, kg·m ⁻³
ρ_n	Normalized density
χ_s	Specific magnetic susceptibility, m ³ ·kg ⁻¹
χ_{s0}	Specific reducing magnetic susceptibility, m ³ ·kg ⁻¹

Subscripts

AGA8-DC92	Calculated from AGA8-DC92 equation of state
EoS	Calculated from an equation of state
exp	Experimental

fluid	fluid
GERG-2008	Calculated from GERG-2008 equation of state
GERG-imp	Calculated from enhanced version of the GERG-2008 equation of state
i	i-th component
j	j-th component
MP	Measuring position
r	Relative
s	Sinker (however, “specific” in case of χ_s and χ_{s0})
T	Overall
Ti	Titanium
Ta	Tantalum
ZP	Zero position

1. Introduction

Hydrogen-enriched natural gas (H2NG) is a blend of natural gas (NG) and hydrogen that is compatible with current NG infrastructure. Injecting hydrogen directly into the NG grid provides an economical solution for transporting and storing hydrogen generated from intermittent renewable energy sources. Furthermore, injecting hydrogen from renewable sources, along with the partial or total substitution of NG with biomethane and/or synthetic methane (e-methane), is seen as a sustainable approach for the progressive decarbonization of heating and power systems [1–3]. While hydrogen can theoretically be mixed with NG, biomethane, or e-methane, in any ratio, mixtures containing up to 20 % hydrogen by volume are considered the most feasible near-term option [4–8].

Several challenges must be resolved before hydrogen can be injected into the NG grid on a large scale [9]. From the perspective of end-use appliances, the combustion characteristics of the gas mixture may change, potentially affecting equipment performance [10–13]. Another critical concern is hydrogen embrittlement, as it can compromise the mechanical integrity of iron and steel pipelines [14–16]. Additionally, the design of systems for the production, transport, and storage of H2NG mixtures, particularly for custody transfer applications, relies heavily on precise and consolidated data for volumetric and calorific properties which usually are derived from reference equations of state (EoS) [17,18].

The AGA8-DC92 [19] and the GERG-2008 [20,21] EoS are established among both industry and academia as reference EoS for NG mixtures. The underlying framework of these EoS is built on experimental data of the constituting pure components and of the consequent binary mixtures. Experimental data on pure NG components and binary mixtures have been essential for developing these EoS and remain crucial for their refinement. [22], especially for binary mixtures of the main components of NG with hydrogen [23–28]. Additionally, high-accuracy experimental thermophysical data from multicomponent H2NG mixtures—prepared with minimal composition uncertainty—are especially valuable for testing the reliability of these equations originally developed for NG mixtures when applied to H2NG mixtures [29–31].

In a recent paper [32], our group evaluated the performance of these reference EoS in predicting the thermophysical properties of a high-calorific NG (H₂-free) mixture composed mainly of methane (> 97 %) and of two derived H2NG mixtures with nominal hydrogen concentrations of 10 % and 20% (mol/mol). We obtained density measurements for these three mixtures at temperatures ranging from (250 to 350) K and pressures up to 20 MPa, using a high-precision single-sinker magnetic suspension densimeter. Overall, the experimental density values for the H₂-free NG mixture aligned well with the predicted values, within the stated uncertainty of the equations. However, for the H2NG mixtures, larger deviations from the predicted densities were observed, particularly at lower temperatures and higher pressures. The maximum relative deviations reached nearly 0.2 %—exceeding the claimed uncertainty of 0.1 % for all three EoS.

In this follow-up work, in a similar way, we offer experimental density data for a new standard high-calorific NG mixture and for two derived H2NG mixtures, also with nominal hydrogen concentration of 10 % and 20 % (mol/mol). In this case, the corresponding initial NG mixture deviates from the initial mixture of the first study [32], with significant amounts of ethane (9 % (mol/mol) compared to 0.4 %) and propane (3 % (mol/mol) compared to 0.2 %), while the content of methane is reduce to 85 % (mol/mol). All investigated mixtures were gravimetrically prepared following ISO 6142-1 [33] to ensure reference quality. The density measurements were conducted using the same high-precision single-sinker densimeter as in the previous work, covering a temperature range from (260 to 350) K and pressures up to 20 MPa. The experimental density results obtained in this study are compared with the aforementioned three reference EoS for NG related mixtures: the AGA8-DC92, the GERG-2008, and an enhanced version of the GERG, referred to in this study as “improved-GERG-2008”.

2. Experimental

2.1. Mixture preparation

Three synthetic NG mixtures were made at the Federal Institute for Materials Research and Testing (BAM, Bundesanstalt für Materialforschung und -prüfung) in Berlin, Germany. These mixtures were labeled G 432 (the H₂-free NG mixture, cylinder no.: 2031-200915), G 455 (the hydrogen-enriched derivative, G 432 + 10 % H₂, 6079-210111), and G 456 (hydrogen-enriched, G 432 + 20 % H₂, 2059-210201). The first mixture, G 432, is an 11-components, H₂-free NG, with methane (85 %) being the matrix component, but with significant amounts of ethane (9 %), propane (3 %), carbon dioxide (1.4 %), and nitrogen (1 %). The derived mixtures, G 455 and G 456, were created by adding hydrogen to G 432, achieving nominal hydrogen concentrations of 10 % and 20 % (mol/mol), respectively.

Each mixture was prepared in 10 dm³ aluminum cylinders using a gravimetric method in accordance with ISO 6142-1 [33], a procedure for the preparation of reference mixtures ensuring minimal uncertainty in composition [32]. The pure components, listed in Table S1, were used directly without further purification to create various premixtures and dilutions in several filling stages. Detailed filling procedures are given in the Supplement. The mass of each gas component was measured using either an electronic comparator balance (Sartorius LA 34000P-0CE) or a high-precision mechanical balance (Volland HCE 25). To validate each target mixture (G 432, G 455, and G 456), two calibration mixtures were independently prepared following BAM's accredited certification protocol, ensuring no correlation between the sample and calibration mixtures. After finishing gravimetric preparation, the gas mixtures were thoroughly homogenized through heating and rolling. The molar compositions (x_i) and their resultant expanded ($k = 2$) uncertainties in absolute terms, $U(x_i)$, are provided in Table 1.

Before shipment to the University of Valladolid (UVa), each mixture underwent composition validation by Gas Chromatography (GC) at BAM, using a multichannel process analyzer (Siemens MAXUM II, Siemens AG). The validation protocol followed the "bracketing" procedure outlined in the ISO 12963 standard [34]. The results are given in Table S3. Further details of this validation method can be found in a previously published paper [31]. The uncertainties in the concentration values of each component in both the studied mixtures and their validation mixtures were determined using the law of propagation of uncertainty, following the guidelines outlined in the Guide to the Expression of Uncertainty in Measurement (GUM) [35].

The molar mass M , normalized density ρ_0 , higher heating value HHV , and Wobbe index W_s for the three gas mixtures, at reference conditions of 288.15 K and 0.101325 MPa, were calculated using the GERG-2008 EoS, included in the REFPROP 10 [36,37] software, based on their normalized compositions. These values are presented in Table 1 as complementary information. The results show that the G 432 mixture is a high-calorific NG blend. When hydrogen is introduced into the mixture, there is a noticeable diminution in normalized density, higher heating value, and Wobbe index, but all variables still remain within the limits to categorize these mixtures as high-calorific NG blends. Specifically, when 10 % hydrogen (G 455) or 20 % hydrogen (G 456) is added to the NG, the higher heating value per unit volume decreases by 7 % and 14 %, respectively, compared to the original G 432 mixture with no hydrogen. The Wobbe index shows smaller changes, decreasing by 2.7 % and 5.4 %, respectively, for G 455 and G 456.

For the critical properties, calculated also by the GERG-2008 EoS by using the Refprop software, the critical point of the H₂-free NG mixture (G 432) occurs at a temperature of 222.4 K and a pressure of 7.2 MPa, with the cricondenthem at 257.4 K and 4.8 MPa, and the cricondenbar at 238.8 K and 7.9 MPa. In the case of the G 455 mixture (G 432 with 10% H₂), the critical point shifts to 215.7 K and 10.0 MPa, the cricondenthem to 257.0 K and 5.4 MPa, and the cricondenbar to 224.1 K and 10.1 MPa. For the G 456 mixture (G 432 with 20% H₂), the critical point is at 217.1 K and 13.6 MPa, the cricondenthem at 256.4 K and 6.1 MPa, and the cricondenbar cannot be computed. It is worth mentioning that neopentane was not

incorporated into the mixture models used in this study; consequently, its contribution was accounted for by adding it to the n-pentane concentration, as recommended by the GERG-2008 Eos.

2.2. Description of the equipment setup and measurement procedure

The experimental procedure in this work was carried out using a single-sinker magnetic suspension densimeter, widely recognized as one of the most accurate methods for determining fluid density across a broad range of temperatures and pressures, and following the same protocol as in the previous study [32]. This setup includes a pressurized diamagnetic cell, within which a monocrystalline silicon sinker with a precisely calibrated volume ($V_s = 226.4440 \pm 0.0026 \text{ cm}^3$) is suspended and surrounded by the sample gas. The buoyant force acting on the sinker is transmitted to a highly sensitive microbalance (XPE205DR, Mettler Toledo GmbH), which is positioned above the cell at ambient pressure and temperature, via a magnetic coupling mechanism. The underlying measurement principles were initially developed by the group of Wagner at the University of Bochum, Germany [38–41], who first implemented them with two-sinker systems with extremely high accuracy, particularly at low densities, by compensating for adsorption effects. This was later implemented to single-sinker systems, which, while simpler, provide equally precise measurements at higher densities [42,43].

The equation used to estimate the density of the fluid is:

$$\rho_{fluid} = \frac{\phi_0 m_s + (m_{Ti} - m_{Ta}) + (W_{ZP} - W_{MP})/\alpha}{V_s(T,p)} \frac{1}{\phi_0} + \frac{\varepsilon_p \chi_s}{\phi_0 \chi_{s0}} \left(\frac{\rho_s}{\rho_0} - \frac{\rho_{fluid}}{\rho_0} \right) \rho_{fluid} \quad (1)$$

where the terms m , V , and ρ denote the mass, volume, and density, respectively, while the subscripts fluid, and s stand for the fluid, and sinker (however, “specific” in case of χ_s and χ_{s0}). The subscripts Ti, and Ta refers to titanium and tantalum counterweights, while ZP, and MP refers to zero and measuring positions of the magnetic coupling. The calibration factor α is determined by weighing two calibrated counterweights of tantalum and titanium, which are alternately placed in the upper pan of the microbalance using an automatic changing device. The counterweights have nearly identical volumes, with their mass difference approximating that of the sinker.

The measurement process is performed by subtracting two separate balance readings. In the zero position (ZP) the electromagnet hanging from the lower hook of the balance pulls the sinker support without raising the sinker, whereas in the measuring position (MP) a greater force is applied to the permanent magnet, fixed to the upper end of the sinker support inside the cell, lifting the silicon sinker. The difference in the balance readings, W , between these two positions effectively cancels out the weights of the sinker support, magnets, and balance hook.

Due to small differences in the vertical positions of the ZP and MP, along with potential instabilities in magnet alignment, the density measurement requires correction for the so-called *force transmission error*. This error consists of two components, namely the apparatus-specific effect and the fluid-specific effect. The apparatus-specific effect is represented by ϕ_0 in Equation (1) and is determined by calculating the sinker weight in vacuum once all the data for an isotherm has been collected. This correction must always be applied to avoid significant errors [44]. The fluid-specific effect, given by the second term on the right-hand side of Equation (1), depends on (a) the specific magnetic susceptibility of the fluid χ_s , (b) the apparatus-specific constant ε_p , and (c) the reducing constants $\chi_{s0} = 10^{-8} \text{ m}^3 \cdot \text{kg}^{-1}$ and $\rho_0 = 1000 \text{ kg} \cdot \text{m}^{-3}$. The value of ε_p was previously determined for our densimeter, along with its dependence on temperature and density, and results were presented in a previous work [45]. Unlike the apparatus-specific effect, the fluid-specific effect is minimal for diamagnetic fluids but can build up a 3% error for paramagnetic fluids, where χ_s can be up to 100 times greater and temperature-dependent [46–48].

The fluid pressure is measured using two quartz crystal transducers: one for low pressures (0–3 MPa) (Digiquartz 2300A-101) and the other for higher pressures (3–20 MPa) (Digiquartz 43KR-HHT-101), both

from Paroscientific Inc. The expanded ($k = 2$) uncertainty for the low-pressure transducer is $U(p) = (6.0 \cdot 10^{-5}(p/\text{MPa}) + 2 \cdot 10^{-3})$ MPa, and for the high-pressure transducer, $U(p) = (7.5 \cdot 10^{-5}(p/\text{MPa}) + 4 \cdot 10^{-3})$ MPa.

The cell temperature is controlled by an oil thermal bath (Dyneo DD-1000F, Julabo GmbH) and an electrical heating cylinder with a temperature controller (MC-E, Julabo GmbH). Temperature is measured, with an expanded ($k = 2$) uncertainty $U(T) = 0.015$ K, by means of two platinum resistance thermometers (SPRT-25, Minco Products Inc.) and an AC resistance bridge (ASL F700, Automatic Systems Laboratory).

A more comprehensive explanation of the equipment and experimental technique is available in earlier publications [49,50].

3. Experimental results

3.1. Measurement uncertainty analysis

The experimental overall expanded ($k = 2$) uncertainty $U_T(\rho_{\text{exp}})$ for the density measurements is presented in Table 2, shown in both absolute and relative terms. This uncertainty accounts for contributions from the density determination uncertainty, $U(\rho_{\text{exp}})$, which has been comprehensively assessed in previous studies [45,50] for our single-sinker densimeter as a function of both density and specific magnetic susceptibility:

$$U(\rho_{\text{exp}})/(\text{kg} \cdot \text{m}^{-3}) = 2.5 \cdot 10^4 \cdot \chi_s/(\text{m}^3 \cdot \text{kg}^{-1}) + 1.1 \cdot 10^{-4} \cdot \rho_{\text{exp}}/(\text{kg} \cdot \text{m}^{-3}) + 2.3 \cdot 10^{-2} \quad (2)$$

combined with the uncertainties from pressure, $u(p)$, temperature, $u(T)$, and composition, $u(x_i)$, following the law of uncertainty propagation [51]:

$$U_T(\rho_{\text{exp}}) = 2 \left[u(\rho_{\text{exp}})^2 + \left(\left. \frac{\partial \rho}{\partial p} \right|_{T,x} u(p) \right)^2 + \left(\left. \frac{\partial \rho}{\partial T} \right|_{p,x} u(T) \right)^2 + \sum_i \left(\left. \frac{\partial \rho}{\partial x_i} \right|_{T,p,x_{j \neq x_i}} u(x_i) \right)^2 \right]^{0.5} \quad (3)$$

The partial derivatives of the mixture density with respect to pressure and temperature are estimated using REFPROP 10 software [36,37], which applies the improved GERG-2008 EoS [52–54]. Here, the most significant contribution to uncertainty arises from $U(p)$ and $U(\rho_{\text{exp}})$, reaching values as high as $0.09 \text{ kg} \cdot \text{m}^{-3}$ (0.44 %). Contributions from $U(x_i)$ and $U(T)$, are much smaller, below $0.017 \text{ kg} \cdot \text{m}^{-3}$ (0.01 %) and $0.0028 \text{ kg} \cdot \text{m}^{-3}$ (0.002 %), respectively. The overall experimental expanded ($k = 2$) uncertainty for the three mixtures varies from (0.031 to 0.096) $\text{kg} \cdot \text{m}^{-3}$, equivalent to 0.033 % to 0.57 %.

3.2. Density measurements

Tables 3, 4, and 5 provide the experimental (p, ρ, T) data for mixtures G 432 (H_2 -free high calorific NG), G 455 (G 432 + 10 % H_2), and G 456 (G 432 + 20 % H_2), the expanded ($k = 2$) uncertainty in density for these measurements calculated using Equation (3), in both absolute and percentage terms, and the relative deviations of the experimental densities from those predicted by the AGA8-DC92 EoS, GERG-2008 EoS, and improved GERG-2008 EoS. Measurements were recorded at five temperatures—260 K, 275 K, 300 K, 325 K, and 350 K—with pressure successively decreasing in 1 MPa steps from 20 MPa down to 1 MPa. Figure 1 presents the data points for the three mixtures, along with the saturation curves calculated from the improved GERG-2008 EoS, the typical operational ranges for pipeline conditions in the gas industry, and the approved application limits for both the AGA8-DC92 and GERG-2008 EoS models.

The AGA8-DC92 EoS [19], developed by the American Gas Association, is a reference model for NG mixtures. Originally formulated as a virial expansion of the compressibility factor, it was later adapted into an explicit Helmholtz energy form to address both calorific and volumetric properties [55]. Its application range covers gas and supercritical phases within (250 to 350) K and up to 30 MPa.

The GERG-2008 EoS [20,21], a model from the Groupe Européen de Recherches Gazières and widely used in Europe, expands the scope of AGA8-DC92 to include liquid and vapor-liquid equilibria (VLE) over a broader range of (60 to 700) K and pressures up to 70 MPa [52]. Both models are capable to describe thermophysical properties of NG mixtures with up to 21 components at pipeline conditions. Their accuracy depends on implemented available experimental data for VLE, density, speed of sound, enthalpy, and heat capacity. To enhance the applicability of GERG-2008 EoS, two major updates were recently made. The first modification targets LNG applications by improving accuracy in the subcooled liquid region from (90 to 180) K up to 10 MPa, using new and reparametrized departure functions for binary mixtures with methane [53]. This adjustment improved density and calorific property predictions for LNG mixtures [56,57]. The second modification specifically focuses on hydrogen-rich mixtures, critical for hydrogen economy processes, by using newer, updated pure-fluid equations and refining binary-specific departure functions [54]. This new approach is able to fix phase envelope issues observed with the original GERG-2008 EoS at low temperatures and reduced deviations in VLE, density, and speed of sound data. Together, these modifications form what we refer to in this study as the “improved GERG-2008” EoS.

4. Discussion

4.1. Relative deviations of experimental data from the reference equations of state

Figures 2, 3, and 4 display the percentage relative deviations of experimental density data from the values calculated using the AGA8-DC92 EoS, GERG-2008 EoS, and improved GERG-2008 EoS models for the G 432, G 455, and G 456 mixtures, respectively. Table 6 presents a statistical comparison of the experimental density data obtained in this study relative to the three EoS models applied. Table 6 also includes the results of the statistical comparison for the three mixtures of our previous work [32]. In Table 6, the statistical indicators are defined as follows: *AARD* (average absolute value of relative deviations), *BiasRD* (average relative deviation), *RMSRD* (root mean square relative deviation), and *MaxRD* (maximum relative deviation), as given by Eqs. (4) to (7):

$$AARD = \frac{1}{N} \sum_{i=1}^N \left| 10^2 \frac{\rho_{i,\text{exp}} - \rho_{i,\text{EoS}}}{\rho_{i,\text{EoS}}} \right| \quad (4)$$

$$BiasRD = \frac{1}{N} \sum_{i=1}^N \left(10^2 \frac{\rho_{i,\text{exp}} - \rho_{i,\text{EoS}}}{\rho_{i,\text{EoS}}} \right) \quad (5)$$

$$RMSRD = \sqrt{\frac{1}{N} \sum_{i=1}^N \left(10^2 \frac{\rho_{i,\text{exp}} - \rho_{i,\text{EoS}}}{\rho_{i,\text{EoS}}} \right)^2} \quad (6)$$

$$MaxRD = \max \left| 10^2 \frac{\rho_{i,\text{exp}} - \rho_{i,\text{EoS}}}{\rho_{i,\text{EoS}}} \right| \quad (7)$$

The density values given by the different EoS were calculated using the normalized composition without impurities given in Table 1. The effect of impurities in the density calculated by the different EoS was estimated to be far below the experimental uncertainty and the deviations.

Relative deviations between the experimental density data for the H₂-free NG mixture (G 432) and the AGA8-DC92 EoS, as shown in Figure 2(a), generally fall within the claimed uncertainty of this EoS ($U(\rho_{\text{EoS}}) = 0.1\%$), except at the lower temperature of 260 K and pressures between 2 and 10 MPa, where deviations

can reach up to -0.15 %. For the same temperature, but at pressures above 9 MPa and up to 16 MPa, deviations between experimental density data and the GERG-2008 EoS increase, reaching -0.21 % (see Figure 2(b)), and are even larger (-0.28%) when compared to the improved GERG-2008 (see Figure 2(c)). For the latter EoS, even at 275 K and pressures above 11 MPa, the density data show deviations exceeding the stated uncertainty, reaching -0.15 %. Notably, this hydrogen-free NG mixture (G 432) contains substantial amounts of ethane and propane. By contrast, results from our previous study [32] on a hydrogen-free NG mixture composed primarily of methane (> 97 %) showed that all three EoS models matched the experimental density data accurately, with maximum relative deviations around 0.05 %.

For the G 455 H₂-enriched NG mixture (G 432 + 10 % H₂), the relative deviations from the three EoS models are shown in Figure 3. In this case, deviations from the AGA8-DC92 EoS (Figure 3(a)) remain within the stated uncertainty of the EoS, except at the lower temperature of 260 K and pressures between 8 MPa and 13 MPa, where positive deviations of up to 0.19 % are observed. At pressures above 19 MPa, slight negative deviations exceeding the stated uncertainty of the EoS can also be seen at a few points at 300 K. Deviations from the GERG-2008 EoS (Figure 3(b)) exceed the claimed uncertainty of the EoS at 260 K for pressures between 4 MPa and 9 MPa (with positive deviations up to 0.20 %) and across all isotherms (except 350 K) for pressures above 12 MPa (260 K, 275 K, and 300 K) and above 17 MPa (325 K), (with negative deviations reaching -0.44 %). Finally, deviations from the improved GERG-2008 EoS (Figure 3(c)) fall within the stated uncertainty only for density data at 350 K. For other isotherms, negative deviations occur for pressures between 5 MPa and 20 MPa, reaching their highest magnitude of -0.38 % for 260 K at around 13 MPa. These results are significantly worse than the equivalent results of our previous work for the 10 % H₂-enriched NG derived from a NG with a significantly higher methane content (G 453) [32], where maximum relative deviations of approximately 0.20 % for any of the three EoS models were observed only at the lowest temperature (which was 250 K in that study).

Figure 4 displays the relative deviations of the experimental density data for the G 456 H₂-enriched NG mixture (G 432 + 20 % H₂) with respect to the three employed EoS models. Similar to the observations for the mixture G 455 (10 % H₂), deviations from the AGA8-DC92 EoS (Figure 4(a)) remain within the stated uncertainty, except at the lower temperature of 260 K and pressures between 7 MPa and 17 MPa, where positive deviations of up to 0.28 % are noted. Likewise, as seen for the G 455 mixture, deviations from the GERG-2008 EoS (Figure 4(b)) exceed the claimed uncertainty at 260 K, with positive deviations up to 0.29 % for pressures below 11 MPa and negative deviations reaching -0.34 % for pressures above 15 MPa. At 300 K, negative deviations up to -0.25 % are observed for pressures above 15 MPa. Finally, deviations from the improved GERG-2008 EoS (Figure 4(c)) fall within the stated uncertainty over the p , T range investigated, except at 260 K (above 11 MPa) and at 300 K (above 8 MPa), where negative deviations reach a maximum of -0.30 %. These deviations are, once again, significantly larger than those from our previous study on 20% H₂-enriched NG derived from the methane-rich gas mixture (G 454) [32], where maximum relative deviations of approximately 0.19% for any of the three EoS models were observed only at the lowest temperature (250 K in that study).

Figures 2 to 4 show that some relative deviations at the lower pressure do not approach zero as expected for ideal gas behavior. This may be due to sorption phenomena, which can slightly alter the mixture's composition and, consequently, the density measurements—particularly in complex mixtures like those studied here. The effects of adsorption and desorption on density measurements of multicomponent gas mixtures were extensively examined by Richter and Kleinrahm [58]. Although our measurement procedure minimizes these effects by evacuating and refilling the cell multiple times, the single-sinker densimeter used here cannot quantify this influence. Nonetheless, we are certain that these deviations are well below the experimental uncertainty, which for technical reasons inherent to the measurement procedure is relatively high at lower pressures and densities, as can be seen from the 'Error bars' on density data in Figures 2 to 4.

The values from the statistical analysis in Table 6 show that the AGA8-DC92 EoS model performs well for the H₂-free NG mixture and slightly less accurately for the 10 % and 20 % H₂-enriched mixtures, as indicated by increasing *AARD* values (0.040 %, 0.048 %, and 0.065 %) and maximum relative deviations (0.15 %, 0.21 %, and 0.28 %).

0.19 %, and 0.28 %) when hydrogen is added. Only a few density data points at the lower temperature (260 K) have deviations exceeding the model's stated uncertainty.

The GERG-2008 and improved GERG-2008 EoS models produce higher deviations for the hydrogen-free mixture (G 432) than the AGA8-DC92, with maximum relative deviations of 0.21 % and 0.28 % compared to 0.15 %. Interestingly, these models handle the 20 % H₂-enriched mixture slightly better than the 10 % H₂-enriched mixture, with *AARD* values of 0.094 % and 0.077 % versus 0.11 % and 0.12 %, and maximum relative deviations (*MarRD*) of 0.34 % and 0.30 % versus 0.44 % and 0.38 %. For the 20 % H₂-enriched mixture, both the GERG and improved GERG models yield results similar to those of the AGA8-DC92 EoS.

Table 6 also includes results for the equivalent mixtures derived from a methane-rich NG of our previous work [32] for comparison. Overall, all three EoS models perform better with those mixtures derived from a NG of higher methane content than with the (methane-depleted) mixtures in this study, which contain significant amounts of heavier hydrocarbons.

4.2. Isothermal compressibility derived from experimental density data

The experimental density values provide additional state properties through their derivatives by applying thermodynamic potentials. Figure 5 shows the partial derivatives of experimental density with respect to pressure, $\left. \frac{\partial \rho_{\text{exp}}}{\partial p} \right|_T$, while Table 7 lists the resultant isothermal compressibility values, $\kappa_T = \frac{1}{\rho_{\text{exp}}} \left. \frac{\partial \rho_{\text{exp}}}{\partial p} \right|_T$, for the three studied mixtures. These derivatives were calculated using cubic spline interpolation on the measured density data, with values at the maximum and minimum pressures of each isotherm excluded from the analysis. As temperature decreases, the partial derivatives exhibit a more convex shape, which flattens as hydrogen content increases across the studied pressure and temperature ranges. The κ_T values span from (0.0361 to 0.5427) MPa⁻¹ at 250 K for the H₂-free NG mixture (G 432), decreasing as both temperature and hydrogen concentration rise. A similar qualitative behavior, with comparable κ_T values, was observed in our previous work [32] for the NG mixture (mainly methane, > 97 %) and the two derived mixtures with 10 % and 20 % hydrogen.

The solid lines in Figure 5, representing the values of $\left. \frac{\partial \rho_{\text{EoS}}}{\partial p} \right|_T$ predicted by the improved GERG-2008 EoS, closely match those values derived from the experimental densities obtained in this work. Statistical analysis of the relative deviations shows *AARD* values of 0.23 %, 0.29 %, and 0.29 % and consequent *MaxRD* values of 1.9 %, 1.6 %, and 1.3 % for the H₂-free (G 432), 10 % H₂ (G 455), and 20 % H₂ (G 456) mixtures, respectively. All deviations are located within the estimated expanded ($k = 2$) uncertainty of κ_T , $U_r(\kappa_T) = 0.7$ %. The same was observed for the mixtures analyzed in our previous work [32], but in that case relative deviations were even smaller with *AARD* values of 0.18 %, 0.14 %, and 0.13 % and *MaxRD* values of 2.0 %, 1.7 %, and 1.3 % for the H₂-free (G 431), 10 % H₂ (G 453) and 20 % H₂ (G 454) mixtures, respectively. Comparison with the other EoS considered in this work gave similar results. Statistical analysis of the relative deviations against values predicted by AGA8-DC92 and GERG-2008 EoS shows *AARD* values below 0.21 % and 0.26 %, and consequent *MaxRD* values below 2.0 % and 1.9 %, respectively, for the three mixtures.

5. Conclusions

This study evaluates the accuracy of reference equations of state (EoS) commonly used for NG when applied to hydrogen-enriched NG (H₂NG) mixtures. To achieve this, density measurements were taken for three synthetic NG-related mixtures across a temperature range of (260 to 350) K and pressures up to 20 MPa, using a high-precision single-sinker magnetic suspension densimeter. The first mixture is a high-calorific,

11-component NG blend with substantial ethane and propane content. The other two mixtures were created by adding hydrogen to the base mixture, resulting in compositions with a nominal hydrogen content of 10 % and 20 % (mol/mol), respectively. All mixtures were gravimetrically prepared to maximize composition accuracy.

The experimental density data was compared to densities predicted by three reference EoS: AGA8-DC92, GERG-2008, and an improved version of GERG-2008. For the H₂-free NG mixture (G 432), AGA8-DC92 generally remained within its stated uncertainty (0.1 %), except at the lowest temperature (260 K) and moderate pressures, while both GERG-2008 and its improved version displayed larger deviations that became more pronounced especially at lower temperatures and higher pressures. For the 10 % H₂-enriched mixture (G 455), AGA8-DC92 mostly remained within its uncertainty range, though it showed some deviation at low temperatures and high pressures. GERG-2008 and improved GERG-2008 exceeded their uncertainty limits (0.1 %) at lower temperatures and some pressure levels, with deviations reaching up to -0.44 %. In the 20 % H₂-enriched mixture (G 456), deviations from all three models exceeded the stated uncertainties at low temperatures and higher pressures, following a similar pattern to the 10% mixture.

AGA8-DC92 exhibited smaller deviations across both H₂-free and H₂-enriched mixtures than the GERG models. Maximum relative deviations increased for the AGA8-DC92 EoS as hydrogen content increased. However, the GERG models showed slightly improved performance for the 20% H₂-enriched mixture over the 10 % mixture. Compared with the findings from our previous study [32], we can say that, in general, EoS models performed best with “simpler”, methane-rich mixtures. However, for mixtures that deviate from this composition, such as those with significant ethane and propane content studied in this work, EoS accuracy decreased, especially at lower temperatures and higher pressures.

Experimental density data for multicomponent H₂NG mixtures are crucial for refining and validating reference EoS models, which are essential for accurate system design, operation, and custody transfer processes. This will become more relevant because a higher diversity in the composition of energy gases can be expected. Experimental data on binary mixtures of ethane or propane with hydrogen remain crucial for the refinement of these EoS.

Acknowledgments

This study was supported by the European Metrology Programme for Innovation and Research (EMPIR), Funder ID: 10.13039/100014132, Grant No. 19ENG03 MefHySto, as well as by the Regional Government of Castilla y León (Junta de Castilla y León), the Ministry of Science and Innovation MCIN, and the European Union NextGenerationEU/PRTR, under project C17.I01.P01.S21.

Figures

Figure 1.

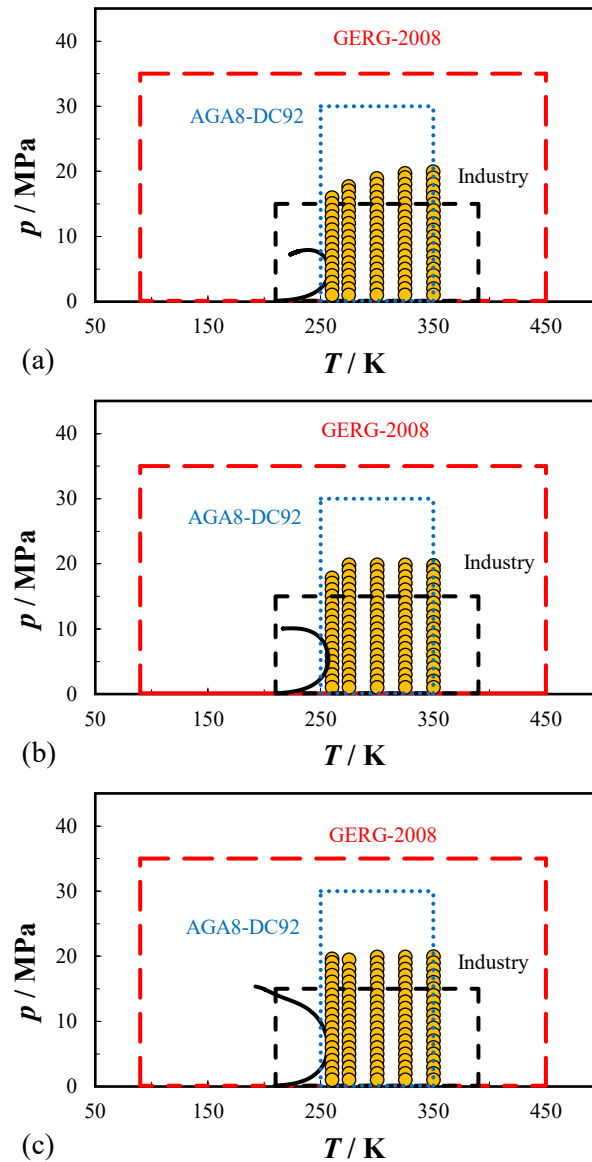


Figure 1. p , T -phase diagram with experimental points (●) and the calculated phase envelope (solid line) using the improved GERG EoS [52–54] for: a) NG mixture G 432 (H_2 -free), b) H₂NG mixture G 455 (10 % H_2), and c) H₂NG gas mixture G 456 (20 % H_2). The marked temperature and pressure ranges indicate the validity of the AGA8-DC92 EoS [19] and GERG-2008 EoS [20,21], as well as the area of interest for the gas industry.

Figure 2.

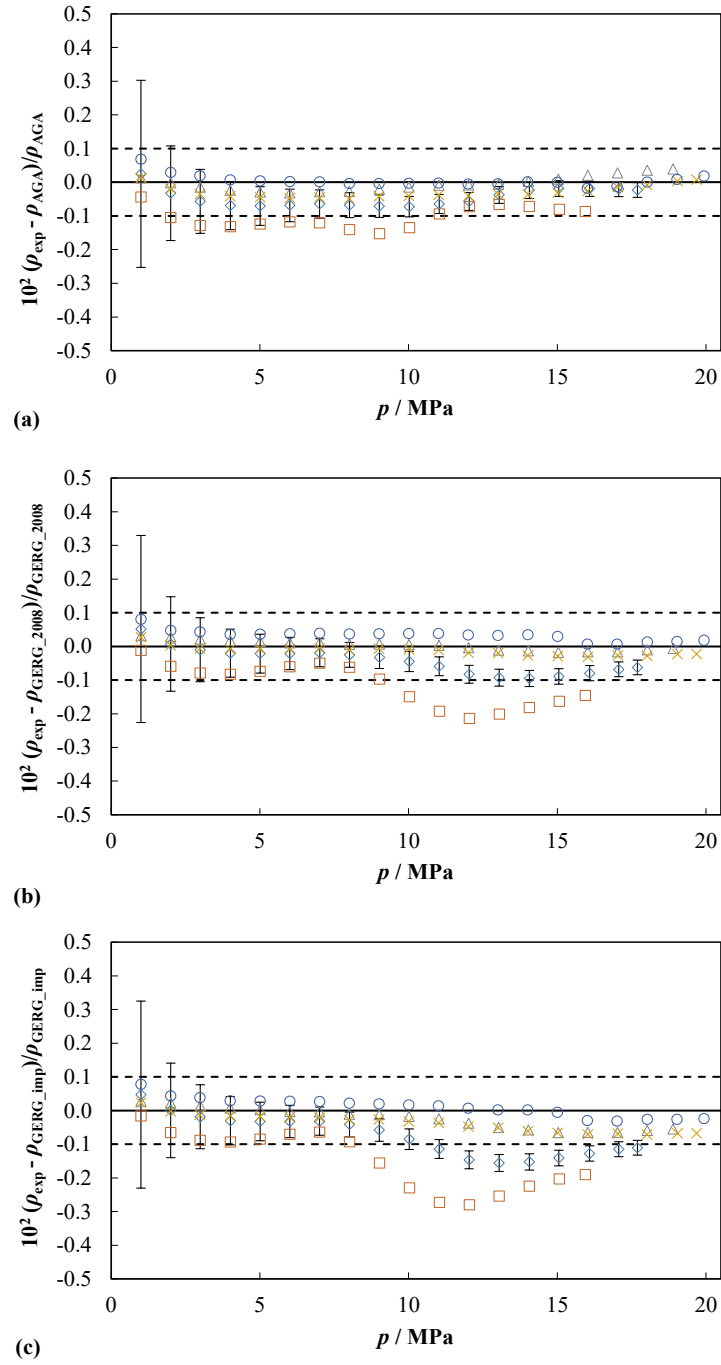


Figure 2. Relative deviations in density of experimental (p, ρ_{exp}, T) data of the (H_2 -free) NG mixture G 432 from density values ρ calculated from (a) AGA8-DC92 EoS [19], (b) GERG-2008 EoS [20,21], and (c) improved GERG-2008 EoS [52–54], as a function of the pressure for different temperatures: \square 260 K, \diamond 275 K, \triangle 300 K, \times 325 K, \circ 350 K. Dashed lines represent the expanded ($k = 2$) uncertainty of the EoS. Error bars on the 275-K data set show the expanded ($k = 2$) uncertainty of the experimental density.

Figure 3.

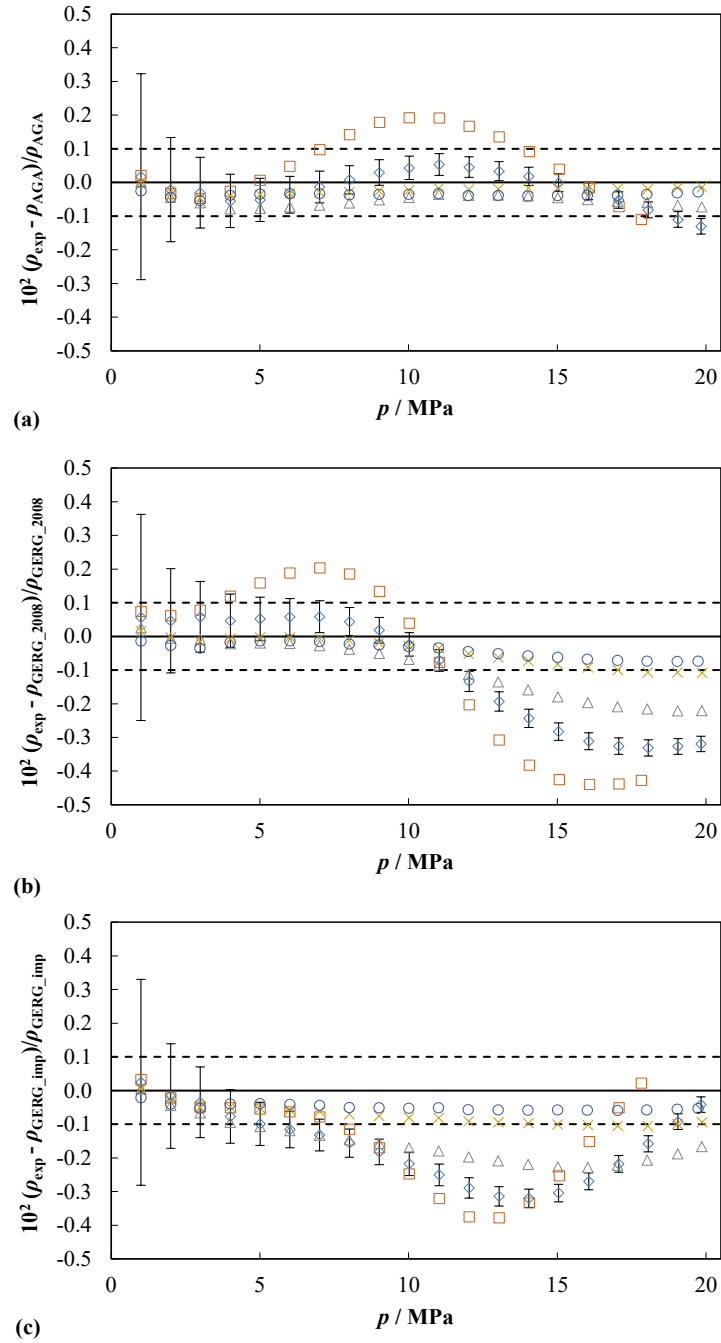


Figure 3. Relative deviations in density of experimental (p, ρ_{exp}, T) data of the H₂NG mixture G 455 (10 % H₂) from density values ρ calculated from (a) AGA8-DC92 EoS [19], (b) GERG-2008 EoS [20,21], and (c) improved GERG-2008 EoS [52–54], as a function of the pressure for different temperatures: \square 260 K, \diamond 275 K, \triangle 300 K, \times 325 K, \circ 350 K. Dashed lines indicate the expanded ($k = 2$) uncertainty of the EoS. Error bars on the 275-K data set show the expanded ($k = 2$) uncertainty of the experimental density.

Figure 4.

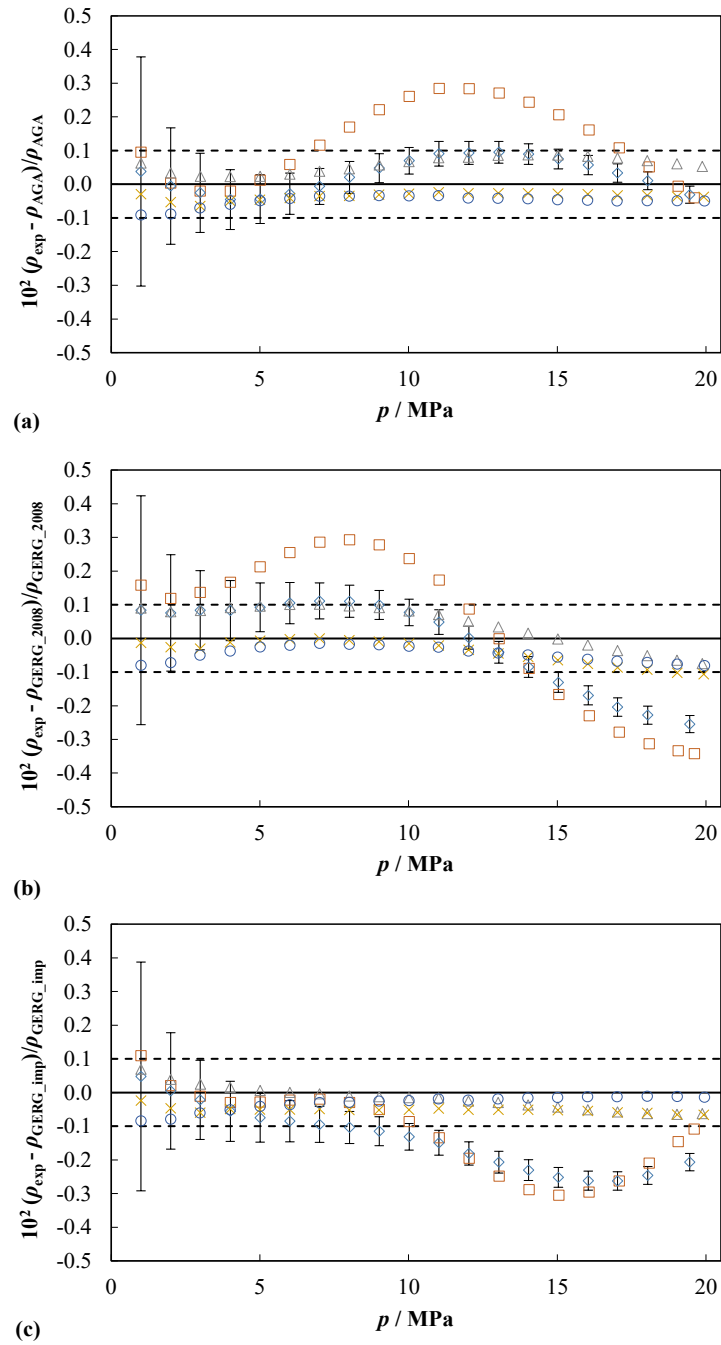


Figure 4. Relative deviations in density of experimental (p, ρ_{exp}, T) data of the H₂NG mixture G 456 (20 % H₂) from density values ρ calculated from (a) AGA8-DC92 EoS [19], (b) GERG-2008 EoS [20,21], and (c) improved GERG-2008 EoS [52–54], as a function of the pressure for different temperatures: \square 260 K, \diamond 275 K, \triangle 300 K, \times 325 K, \circ 350 K. Dashed lines indicate the expanded ($k = 2$) uncertainty of the EoS. Error bars on the 275-K data set show the expanded ($k = 2$) uncertainty of the experimental density.

Figure 5.

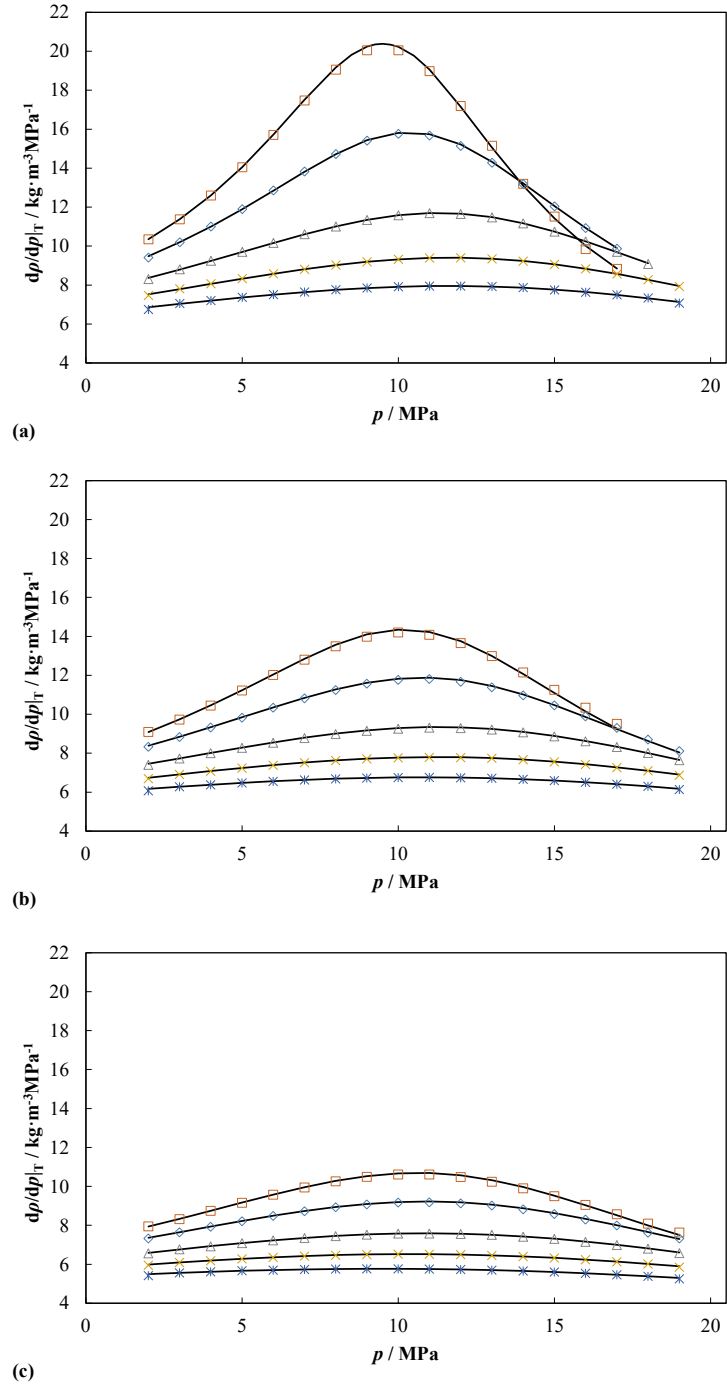


Figure 5. Derived $\left. \frac{\partial \rho_{\text{exp}}}{\partial p} \right|_T$ values of (a) G 432, (b) G 455 (10 % H₂), and (c) G 456 (20 % H₂) mixtures as a function of the pressure for different temperatures: \square 260 K, \diamond 275 K, \triangle 300 K, \times 325 K, \circ 350 K. Solid lines indicate the $\left. \frac{\partial \rho_{\text{EoS}}}{\partial p} \right|_T$ values calculated from the improved GERG-2008 EoS [52–54].

Tables

Table 1. Composition of the reference NG mixtures studied in this work, with impurity compounds indicated in *italics*.

Component	G 432		G 455 (G 432 + 10 % H ₂)		G 456 (G 432 + 20 % H ₂)	
	BAM no: 2031-200915		BAM no: 6079-210111		BAM no: 2059-210201	
	10 ² x_i / mol/mol	10 ² $U(x_i)$ / mol/mol	10 ² x_i / mol/mol	10 ² $U(x_i)$ / mol/mol	10 ² x_i / mol/mol	10 ² $U(x_i)$ / mol/mol
Methane	85.0063	0.0026	76.5104	0.0031	68.0159	0.0027
Hydrogen	–	–	9.9864	0.0027	20.0039	0.0046
Nitrogen	0.95080	0.00018	0.85506	0.00016	0.76016	0.00015
Carbon dioxide	1.44823	0.00016	1.30441	0.00016	1.16003	0.00015
Ethane	8.99177	0.00072	8.11044	0.00073	7.18322	0.00072
Propane	3.00256	0.00051	2.69314	0.00051	2.39645	0.00050
<i>n</i> -Butane	0.19994	0.00012	0.18016	0.00010	0.160109	0.000091
Isobutane	0.200443	0.000074	0.180025	0.000059	0.160276	0.000053
<i>n</i> -Pentane	0.050054	0.000021	0.044993	0.000018	0.040018	0.000016
Isopentane	0.049929	0.000020	0.044914	0.000018	0.039882	0.000016
Neopentane	0.050035	0.000031	0.045022	0.000028	0.040009	0.000025
<i>n</i> -Hexane	0.049965	0.000016	0.044995	0.000014	0.039986	0.000013
<i>Oxygen</i>	<i>0.0000120</i>	<i>0.0000070</i>	<i>0.0000130</i>	<i>0.0000061</i>	<i>0.0000150</i>	<i>0.0000078</i>

<i>Hydrogen</i>	0.0000020	0.0000011	-	-	-	-
<i>Carbon monoxide</i>	0.00000100	0.00000078	0.0000020	0.0000014	0.0000030	0.0000026
<i>Propene</i>	0.0000030	0.0000035	0.0000030	0.0000035	0.0000020	0.0000023
<i>Ethylene</i>	0.0000010	0.0000012	0.0000010	0.0000012	0.0000010	0.0000012
<i>Nitric oxide</i>	0.00000010	0.00000012	0.00000010	0.00000012	0.00000010	0.00000012

Normalized composition without impurities

Methane	85.0063	0.0026	76.5104	0.0031	68.0159	0.0027
Hydrogen	-	-	9.9864	0.0027	20.0039	0.0046
Nitrogen	0.95080	0.00018	0.85506	0.00016	7.18322	0.00072
Carbon dioxide	1.44823	0.00016	1.30441	0.00016	2.39645	0.00050
Ethane	8.99177	0.00072	8.11044	0.00073	1.16003	0.00015
Propane	3.00256	0.00051	2.69314	0.00051	0.76016	0.00015
<i>n</i> -Butane	0.19994	0.00012	0.18016	0.00010	0.160276	0.000053
Isobutane	0.200443	0.000074	0.180025	0.000059	0.160109	0.000091
<i>n</i> -Pentane	0.050054	0.000021	0.044993	0.000018	0.040018	0.000016
Isopentane	0.049929	0.000020	0.044914	0.000018	0.040009	0.000025
<i>n</i> -Hexane	0.049965	0.000016	0.044995	0.000014	0.039882	0.000016
Neopentane	0.050035	0.000031	0.045022	0.000028	0.039986	0.000013

Molar mass M g / mol	18.954	17.260	15.566
Normalized density ρ_n kg / m ³	0.80379	0.73154	0.65940
Higher Heating Value HHV MJ / m ³	41.726	38.744	35.768
Wobbe index W_s MJ / m ³	51.523	50.148	48.763

Table 2. Contributions to the overall expanded ($k = 2$) uncertainty in density, $U_T(\rho_{\text{exp}})$, for the three reference NG mixtures examined in this study.

Source	Contribution ($k = 2$)	Units	Estimation in density ($k = 2$)	
			$\text{kg}\cdot\text{m}^{-3}$	%
G 432				
Temperature, T	0.015	K	< 0.0028	< 0.0019
Pressure, p	< 0.005	MPa	(0.023–0.086)	(0.020–0.37)
Composition, x_i	< 0.0004	$\text{mol}\cdot\text{mol}^{-1}$	< 0.011	< 0.0065
Density, ρ	(0.024–0.050)	$\text{kg}\cdot\text{m}^{-3}$	(0.024–0.050)	(0.021–0.036)
Sum			(0.033–0.096)	(0.030–0.50)
G 455 (G 432 + 10 % H ₂)				
Temperature, T	0.015	K	< 0.0022	< 0.0018
Pressure, p	< 0.005	MPa	(0.022–0.062)	(0.020–0.37)
Composition, x_i	< 0.0004	$\text{mol}\cdot\text{mol}^{-1}$	< 0.015	< 0.0088
Density, ρ	(0.024–0.046)	$\text{kg}\cdot\text{m}^{-3}$	(0.024–0.046)	(0.023–0.039)
Sum			(0.032–0.073)	(0.031–0.53)
G 456 (G 432 + 20 % H ₂)				
Temperature, T	0.015	K	< 0.0018	< 0.0016
Pressure, p	< 0.005	MPa	(0.019–0.047)	(0.020–0.37)
Composition, x_i	< 0.0004	$\text{mol}\cdot\text{mol}^{-1}$	< 0.017	< 0.010
Density, ρ	(0.023–0.043)	$\text{kg}\cdot\text{m}^{-3}$	(0.023–0.043)	(0.024–0.44)
Sum			(0.031–0.061)	(0.033–0.57)

Table 3. Experimental (p, ρ_{exp}, T) measurements for the (H_2 -free) NG mixture G 432, absolute and relative expanded ($k = 2$) uncertainty in density, $U(\rho_{\text{exp}})$, relative deviations from the density given by the AGA8-DC92 EoS [19], $\rho_{\text{AGA8-DC92}}$, the GERG-2008 EoS [20,21], $\rho_{\text{GERG-2008}}$, and the improved GERG-2008 EoS [52–54], $\rho_{\text{GERG-improved}}$.

$T / \text{K}^{(a)}$	$p / \text{MPa}^{(a)}$	$\rho_{\text{exp}} / \text{kg} \cdot \text{m}^{-3(a)}$	$U(\rho_{\text{exp}}) / \text{kg} \cdot \text{m}^{-3}$	$10^2 U(\rho_{\text{exp}}) / \rho_{\text{exp}}$	$10^2 (\rho_{\text{exp}} - \rho_{\text{AGA8-DC92}}) / \rho_{\text{AGA8-DC92}}$	$10^2 (\rho_{\text{exp}} - \rho_{\text{GERG-2008}}) / \rho_{\text{GERG-2008}}$	$10^2 (\rho_{\text{exp}} - \rho_{\text{GERG-improved}}) / \rho_{\text{GERG-improved}}$
260.000 K							
260.172	15.94387	234.701	0.050	0.021	-0.087	-0.146	-0.190
260.173	15.06566	225.286	0.049	0.022	-0.081	-0.163	-0.203
260.173	14.06213	213.074	0.047	0.022	-0.072	-0.182	-0.224
260.172	13.04828	198.893	0.046	0.023	-0.067	-0.201	-0.254
260.171	12.04212	182.780	0.044	0.024	-0.073	-0.214	-0.280
260.174	11.03616	164.678	0.042	0.025	-0.094	-0.193	-0.272
260.171	10.03085	145.054	0.039	0.027	-0.135	-0.149	-0.230
260.171	9.02392	124.786	0.037	0.030	-0.153	-0.097	-0.155
260.173	8.01756	105.026	0.035	0.033	-0.141	-0.062	-0.093
260.173	7.01074	86.610	0.033	0.038	-0.120	-0.050	-0.064
260.173	6.00939	70.010	0.031	0.044	-0.118	-0.060	-0.070
260.175	5.00703	55.129	0.029	0.053	-0.125	-0.074	-0.085
260.174	4.00615	41.834	0.028	0.066	-0.132	-0.083	-0.093
260.176	2.99405	29.750	0.026	0.088	-0.129	-0.079	-0.088
260.170	2.00451	19.044	0.025	0.132	-0.105	-0.059	-0.065
260.180	1.00292	9.138	0.024	0.262	-0.044	-0.012	-0.016
275.000 K							
275.061	17.69592	221.059	0.048	0.022	-0.023	-0.063	-0.110
275.061	17.06480	215.039	0.047	0.022	-0.020	-0.068	-0.115
275.060	16.08785	204.939	0.046	0.023	-0.019	-0.080	-0.127
275.060	15.05121	193.104	0.045	0.023	-0.019	-0.089	-0.141
275.060	14.05879	180.626	0.043	0.024	-0.024	-0.095	-0.152
275.061	13.04325	166.705	0.042	0.025	-0.038	-0.093	-0.155
275.059	12.03336	151.847	0.040	0.026	-0.057	-0.083	-0.146
275.060	11.02685	136.321	0.038	0.028	-0.065	-0.059	-0.114
275.059	10.02282	120.507	0.037	0.030	-0.073	-0.045	-0.085
275.059	9.01787	104.818	0.035	0.033	-0.071	-0.032	-0.058
275.058	8.01330	89.673	0.033	0.037	-0.068	-0.025	-0.041
275.059	7.01084	75.371	0.031	0.042	-0.065	-0.019	-0.031
275.059	6.00932	62.022	0.030	0.048	-0.069	-0.021	-0.032
275.060	5.00667	49.629	0.029	0.058	-0.070	-0.021	-0.032
275.059	4.00525	38.178	0.027	0.071	-0.069	-0.020	-0.030
275.058	2.99255	27.463	0.026	0.095	-0.057	-0.010	-0.018
275.058	2.00274	17.741	0.025	0.140	-0.033	0.007	0.001
275.060	1.00263	8.587	0.024	0.278	0.025	0.052	0.047
300.000 K							
300.052	18.89613	191.689	0.045	0.023	0.039	-0.006	-0.054
300.053	18.02313	183.947	0.044	0.024	0.035	-0.010	-0.059
300.050	17.02221	174.545	0.043	0.025	0.027	-0.016	-0.065
300.052	16.02865	164.658	0.042	0.025	0.021	-0.016	-0.065
300.048	15.03453	154.249	0.040	0.026	0.009	-0.018	-0.065
300.050	14.02944	143.258	0.039	0.027	0.003	-0.013	-0.057
300.048	13.02806	131.933	0.038	0.029	-0.006	-0.011	-0.050
300.052	12.02303	120.313	0.037	0.030	-0.008	-0.004	-0.037

300.046	11.01692	108.579	0.035	0.032	-0.009	0.003	-0.024
300.048	10.01484	96.916	0.034	0.035	-0.015	0.005	-0.017
300.047	9.01055	85.404	0.033	0.038	-0.021	0.007	-0.012
300.042	8.01027	74.223	0.031	0.042	-0.028	0.006	-0.011
300.042	7.00785	63.392	0.030	0.048	-0.029	0.011	-0.004
300.041	6.00685	52.999	0.029	0.055	-0.032	0.010	-0.003
300.048	5.00506	43.053	0.028	0.065	-0.029	0.014	0.003
300.050	4.00406	33.577	0.027	0.080	-0.024	0.018	0.008
300.061	2.99033	24.441	0.026	0.105	-0.015	0.022	0.015
300.059	2.00230	15.968	0.025	0.155	-0.001	0.028	0.022
299.994	1.00209	7.801	0.024	0.305	0.013	0.032	0.028
325.000 K							
325.008	19.68452	168.816	0.042	0.025	0.008	-0.023	-0.067
325.013	19.03937	163.762	0.042	0.025	0.004	-0.023	-0.067
325.013	18.01498	155.457	0.041	0.026	-0.008	-0.029	-0.071
325.020	17.03292	147.195	0.040	0.027	-0.015	-0.027	-0.068
325.016	16.02401	138.423	0.039	0.028	-0.026	-0.031	-0.070
325.018	15.01422	129.394	0.038	0.029	-0.032	-0.029	-0.066
325.020	14.01120	120.224	0.037	0.030	-0.036	-0.027	-0.061
325.028	13.01072	110.933	0.036	0.032	-0.035	-0.020	-0.051
325.025	12.00972	101.554	0.034	0.034	-0.041	-0.019	-0.048
325.025	11.01092	92.178	0.033	0.036	-0.038	-0.011	-0.037
325.028	10.00864	82.804	0.032	0.039	-0.040	-0.009	-0.032
325.031	9.00811	73.544	0.031	0.043	-0.042	-0.006	-0.027
325.022	8.00796	64.437	0.030	0.047	-0.048	-0.010	-0.028
325.022	7.00712	55.515	0.029	0.053	-0.046	-0.006	-0.021
325.021	6.00600	46.809	0.028	0.060	-0.047	-0.008	-0.020
325.020	5.00509	38.351	0.027	0.071	-0.045	-0.008	-0.017
325.017	4.00388	30.149	0.026	0.087	-0.042	-0.008	-0.016
325.023	2.98813	22.100	0.025	0.115	-0.036	-0.007	-0.013
325.033	2.00275	14.555	0.025	0.169	-0.020	0.003	-0.002
325.039	1.00275	7.160	0.024	0.331	0.012	0.027	0.023
350.000 K							
350.025	19.92958	149.082	0.040	0.027	0.018	0.018	-0.024
350.028	19.02344	142.700	0.039	0.027	0.008	0.015	-0.026
350.036	18.02717	135.497	0.038	0.028	< 0.001	0.014	-0.026
350.030	17.00874	127.951	0.037	0.029	-0.013	0.007	-0.031
350.034	16.00839	120.379	0.037	0.030	-0.018	0.007	-0.030
350.081	15.00598	112.656	0.036	0.032	< 0.001	0.030	-0.005
350.091	14.00636	104.848	0.035	0.033	0.001	0.035	0.002
350.086	13.00643	96.959	0.034	0.035	-0.005	0.033	0.002
350.089	12.00505	89.014	0.033	0.037	-0.005	0.034	0.007
350.088	11.00552	81.075	0.032	0.040	-0.002	0.039	0.014
350.091	10.00554	73.146	0.031	0.043	-0.003	0.038	0.017
350.091	9.00400	65.256	0.030	0.046	-0.004	0.038	0.020
350.091	8.00542	57.467	0.029	0.051	-0.004	0.037	0.022
350.092	7.00527	49.769	0.029	0.057	0.001	0.039	0.027
350.094	6.00494	42.191	0.028	0.066	0.002	0.038	0.028
350.093	5.00447	34.753	0.027	0.077	0.004	0.036	0.029
350.093	4.00306	27.461	0.026	0.095	0.007	0.035	0.029
350.095	2.98569	20.223	0.025	0.125	0.019	0.043	0.038
350.095	2.00252	13.394	0.024	0.182	0.029	0.048	0.044
350.095	1.00263	6.621	0.024	0.357	0.069	0.081	0.078

^(a) Expanded uncertainties ($k = 2$): $U(p > 3)/\text{MPa} = 7.5 \cdot 10^{-5} \cdot \frac{p}{\text{MPa}} + 4 \cdot 10^{-3}$; $U(p < 3)/\text{MPa} = 6.0 \cdot$

$10^{-5} \cdot \frac{p}{\text{MPa}} + 2 \cdot 10^{-3}$; $U(T) = 15 \text{ mK}$; $\frac{U(\rho)}{\text{kg}\cdot\text{m}^{-3}} = 2.5 \cdot 10^4 \frac{\chi_S}{\text{m}^3\text{kg}^{-1}} + 1.1 \cdot 10^{-4} \cdot \frac{\rho}{\text{kg}\cdot\text{m}^{-3}} + 2.3 \cdot 10^{-2}$.

Table 4. Experimental (p , ρ_{exp} , T) measurements for the (H_2 -enriched) NG mixture G 455 (10 % H_2), absolute and relative expanded ($k = 2$) uncertainty in density, $U(\rho_{\text{exp}})$, relative deviations from the density given by the AGA8-DC92 EoS [19], $\rho_{\text{AGA8-DC92}}$, the GERG-2008 EoS [20,21], $\rho_{\text{GERG-2008}}$, and the improved GERG-2008 EoS [52–54], $\rho_{\text{GERG-improved}}$.

$T / \text{K}^{(a)}$	$p / \text{MPa}^{(a)}$	$\rho_{\text{exp}} / \text{kg} \cdot \text{m}^{-3(a)}$	$U(\rho_{\text{exp}}) / \text{kg} \cdot \text{m}^{-3}$	$10^2 U(\rho_{\text{exp}}) / \rho_{\text{exp}}$	$10^2 (\rho_{\text{exp}} - \rho_{\text{AGA8-DC92}}) / \rho_{\text{AGA8-DC92}}$	$10^2 (\rho_{\text{exp}} - \rho_{\text{GERG-2008}}) / \rho_{\text{GERG-2008}}$	$10^2 (\rho_{\text{exp}} - \rho_{\text{GERG-improved}}) / \rho_{\text{GERG-improved}}$
260.000 K							
260.175	17.82969	206.100	0.046	0.023	-0.110	-0.427	0.022
260.176	17.07126	199.200	0.046	0.023	-0.071	-0.438	-0.051
260.178	16.07939	189.459	0.044	0.023	-0.016	-0.440	-0.151
260.176	15.06483	178.600	0.043	0.024	0.040	-0.425	-0.253
260.177	14.05752	166.893	0.042	0.025	0.092	-0.383	-0.333
260.177	13.04719	154.256	0.040	0.026	0.136	-0.308	-0.378
260.177	12.03347	140.786	0.039	0.028	0.167	-0.203	-0.375
260.177	11.03276	126.920	0.037	0.029	0.192	-0.077	-0.321
260.178	10.02125	112.602	0.036	0.032	0.192	0.039	-0.247
260.182	9.01879	98.457	0.034	0.035	0.179	0.134	-0.170
260.179	8.01531	84.655	0.033	0.038	0.142	0.186	-0.114
260.180	7.01157	71.449	0.031	0.043	0.098	0.203	-0.078
260.179	6.00996	59.015	0.030	0.050	0.048	0.189	-0.063
260.178	5.00795	47.378	0.028	0.060	0.007	0.159	-0.055
260.179	4.00498	36.523	0.027	0.074	-0.026	0.120	-0.051
260.178	2.99199	26.321	0.026	0.098	-0.047	0.078	-0.048
260.180	2.00384	17.046	0.025	0.146	-0.033	0.061	-0.022
260.181	1.00333	8.264	0.024	0.288	0.021	0.074	0.033
275.000 K							
275.149	19.83024	198.637	0.046	0.023	-0.131	-0.319	-0.042
275.149	19.05955	192.537	0.045	0.023	-0.110	-0.327	-0.092
275.149	18.05989	184.137	0.044	0.024	-0.082	-0.331	-0.158
275.150	17.06344	175.188	0.043	0.024	-0.052	-0.326	-0.218
275.150	16.05558	165.537	0.042	0.025	-0.026	-0.311	-0.270
275.152	15.04279	155.246	0.041	0.026	-0.001	-0.283	-0.304
275.151	14.04366	144.550	0.039	0.027	0.018	-0.243	-0.320
275.152	13.04090	133.347	0.038	0.029	0.034	-0.193	-0.314
275.153	12.03273	121.726	0.037	0.030	0.046	-0.134	-0.289
275.153	11.02767	109.934	0.035	0.032	0.053	-0.071	-0.250
275.151	10.02315	98.095	0.034	0.035	0.043	-0.024	-0.217
275.151	9.01456	86.332	0.033	0.038	0.030	0.018	-0.182
275.149	8.01243	74.910	0.031	0.042	0.008	0.044	-0.156
275.148	7.00879	63.851	0.030	0.047	-0.013	0.058	-0.132
275.148	6.00792	53.274	0.029	0.054	-0.036	0.058	-0.116
275.148	5.00582	43.180	0.028	0.064	-0.052	0.052	-0.099
275.150	4.00504	33.606	0.027	0.079	-0.055	0.046	-0.077
275.153	2.99096	24.415	0.026	0.105	-0.030	0.058	-0.035
275.150	2.00416	15.931	0.025	0.155	-0.021	0.046	-0.016
275.153	1.00349	7.771	0.024	0.306	0.017	0.056	0.025
300.000 K							
300.098	19.86189	167.813	0.042	0.025	-0.072	-0.220	-0.166
300.097	19.04526	161.669	0.041	0.026	-0.067	-0.221	-0.188
300.098	18.02223	153.661	0.040	0.026	-0.059	-0.215	-0.207
300.095	17.02152	145.498	0.039	0.027	-0.056	-0.209	-0.222

300.095	16.02262	137.045	0.039	0.028	-0.051	-0.197	-0.228	
300.096	15.02094	128.298	0.038	0.029	-0.045	-0.179	-0.226	
300.096	14.02039	119.331	0.036	0.031	-0.040	-0.158	-0.219	
300.097	13.01449	110.137	0.035	0.032	-0.037	-0.135	-0.209	
300.097	12.01914	100.924	0.034	0.034	-0.037	-0.113	-0.197	
300.097	11.01575	91.591	0.033	0.036	-0.035	-0.085	-0.179	
300.098	10.01397	82.283	0.032	0.039	-0.044	-0.068	-0.170	
300.099	9.01304	73.068	0.031	0.043	-0.051	-0.050	-0.157	
300.096	8.00923	63.965	0.030	0.047	-0.061	-0.038	-0.146	
300.096	7.00832	55.076	0.029	0.053	-0.067	-0.027	-0.133	
300.100	6.00560	46.394	0.028	0.061	-0.072	-0.021	-0.119	
300.100	5.00492	37.982	0.027	0.072	-0.076	-0.020	-0.107	
300.099	4.00431	29.837	0.026	0.088	-0.078	-0.022	-0.095	
300.098	2.98941	21.862	0.025	0.116	-0.060	-0.010	-0.066	
300.099	2.00304	14.382	0.025	0.171	-0.045	-0.005	-0.044	
300.103	1.00294	7.070	0.024	0.335	0.001	0.025	0.005	
				325.000 K				
325.097	19.86308	145.342	0.039	0.027	-0.014	-0.109	-0.094	
325.097	19.04171	139.754	0.039	0.028	-0.015	-0.107	-0.099	
325.097	18.04301	132.773	0.038	0.029	-0.020	-0.107	-0.106	
325.095	17.03409	125.540	0.037	0.030	-0.018	-0.100	-0.105	
325.095	16.03472	118.203	0.036	0.031	-0.018	-0.092	-0.103	
325.095	15.01273	110.548	0.035	0.032	-0.017	-0.083	-0.100	
325.093	14.02712	103.047	0.035	0.034	-0.017	-0.073	-0.097	
325.093	13.02177	95.305	0.034	0.035	-0.019	-0.062	-0.094	
325.093	12.02022	87.533	0.033	0.038	-0.021	-0.052	-0.091	
325.093	11.01652	79.725	0.032	0.040	-0.017	-0.035	-0.081	
325.094	10.01210	71.912	0.031	0.043	-0.023	-0.028	-0.080	
325.093	9.00774	64.144	0.030	0.047	-0.025	-0.019	-0.075	
325.095	8.00864	56.486	0.029	0.052	-0.028	-0.012	-0.070	
325.095	7.00809	48.915	0.028	0.058	-0.029	-0.004	-0.062	
325.095	6.00585	41.448	0.028	0.067	-0.032	-0.002	-0.057	
325.095	5.00480	34.129	0.027	0.078	-0.036	-0.003	-0.052	
325.096	4.00386	26.964	0.026	0.096	-0.039	-0.007	-0.049	
325.099	2.98777	19.857	0.025	0.127	-0.045	-0.016	-0.049	
325.099	2.00334	13.144	0.024	0.186	-0.027	-0.003	-0.027	
325.102	1.00308	6.494	0.024	0.364	0.001	0.016	0.004	
				350.000 K				
350.086	19.73559	127.910	0.037	0.029	-0.027	-0.074	-0.053	
350.086	19.03490	123.623	0.037	0.030	-0.031	-0.074	-0.055	
350.086	18.01221	117.253	0.036	0.031	-0.035	-0.073	-0.057	
350.087	17.02173	110.962	0.036	0.032	-0.038	-0.072	-0.058	
350.088	16.01177	104.441	0.035	0.033	-0.039	-0.067	-0.058	
350.089	15.01162	97.891	0.034	0.035	-0.039	-0.062	-0.058	
350.087	14.01032	91.255	0.033	0.036	-0.040	-0.058	-0.058	
350.088	13.01344	84.590	0.033	0.038	-0.039	-0.051	-0.057	
350.087	12.00734	77.821	0.032	0.041	-0.038	-0.045	-0.057	
350.087	11.00656	71.069	0.031	0.044	-0.033	-0.034	-0.051	
350.088	10.00614	64.310	0.030	0.047	-0.035	-0.031	-0.052	
350.085	9.00469	57.562	0.029	0.051	-0.035	-0.025	-0.051	
350.087	8.00657	50.867	0.029	0.056	-0.036	-0.022	-0.050	
350.086	7.00340	44.191	0.028	0.063	-0.032	-0.016	-0.044	
350.095	6.00561	37.612	0.027	0.072	-0.032	-0.013	-0.041	
350.097	5.00391	31.086	0.026	0.085	-0.034	-0.013	-0.039	
350.096	4.00402	24.661	0.026	0.104	-0.038	-0.017	-0.039	

350.092	2.98364	18.205	0.025	0.137	-0.054	-0.035	-0.052
350.093	2.00254	12.108	0.024	0.200	-0.043	-0.027	-0.040
350.086	1.00257	6.004	0.024	0.393	-0.025	-0.014	-0.021

^(a) Expanded uncertainties ($k = 2$): $U(p > 3)/\text{MPa} = 7.5 \cdot 10^{-5} \cdot \frac{p}{\text{MPa}} + 4 \cdot 10^{-3}$; $U(p < 3)/\text{MPa} = 6.0 \cdot$

$$10^{-5} \cdot \frac{p}{\text{MPa}} + 2 \cdot 10^{-3}; U(T) = 15 \text{ mK}; \frac{U(\rho)}{\text{kg} \cdot \text{m}^{-3}} = 2.5 \cdot 10^4 \frac{\chi_s}{\text{m}^3 \text{kg}^{-1}} + 1.1 \cdot 10^{-4} \cdot \frac{\rho}{\text{kg} \cdot \text{m}^{-3}} + 2.3 \cdot 10^{-2}.$$

Table 5. Experimental (p , ρ_{exp} , T) measurements for the (H₂-enriched) NG mixture G 456 (20 % H₂), absolute and relative expanded ($k = 2$) uncertainty in density, $U(\rho_{\text{exp}})$, relative deviations from the density given by the AGA8-DC92 EoS [19], $\rho_{\text{AGA8-DC92}}$, the GERG-2008 EoS [20,21], $\rho_{\text{GERG-2008}}$, and the improved GERG-2008 EoS [52–54], $\rho_{\text{GERG-improved}}$.

$T / \text{K}^{(a)}$	$p / \text{MPa}^{(a)}$	$\rho_{\text{exp}} / \text{kg}\cdot\text{m}^{-3(a)}$	$U(\rho_{\text{exp}}) / \text{kg}\cdot\text{m}^{-3}$	$10^2 U(\rho_{\text{exp}})/\rho_{\text{exp}}$	$10^2 (\rho_{\text{exp}} - \rho_{\text{AGA8-DC92}})/\rho_{\text{AGA8-DC92}}$	$10^2 (\rho_{\text{exp}} - \rho_{\text{GERG-2008}})/\rho_{\text{GERG-2008}}$	$10^2 (\rho_{\text{exp}} - \rho_{\text{GERG-improved}})/\rho_{\text{GERG-improved}}$
260.000 K							
260.174	19.60635	180.852	0.043	0.024	-0.041	-0.343	-0.108
260.176	19.06388	176.807	0.043	0.024	-0.006	-0.334	-0.145
260.176	18.08779	169.185	0.042	0.025	0.051	-0.313	-0.210
260.177	17.08145	160.855	0.041	0.026	0.108	-0.279	-0.262
260.176	16.07121	152.011	0.040	0.026	0.161	-0.230	-0.296
260.174	15.05336	142.618	0.039	0.027	0.206	-0.166	-0.305
260.176	14.04961	132.913	0.038	0.029	0.244	-0.089	-0.288
260.177	13.04327	122.804	0.037	0.030	0.271	-0.001	-0.248
260.176	12.03722	112.398	0.036	0.032	0.284	0.087	-0.195
260.174	11.02706	101.759	0.034	0.034	0.284	0.173	-0.134
260.177	10.02106	91.082	0.033	0.037	0.261	0.237	-0.086
260.177	9.01720	80.487	0.032	0.040	0.221	0.278	-0.050
260.178	8.01319	70.064	0.031	0.044	0.169	0.293	-0.030
260.178	7.01101	59.936	0.030	0.050	0.116	0.286	-0.019
260.176	6.00829	50.148	0.029	0.057	0.059	0.255	-0.023
260.177	5.00601	40.759	0.028	0.068	0.012	0.212	-0.028
260.177	4.00470	31.797	0.027	0.083	-0.020	0.166	-0.030
260.174	2.99387	23.178	0.026	0.110	-0.020	0.137	-0.011
260.172	2.00318	15.134	0.025	0.163	0.003	0.119	0.021
260.178	1.00301	7.400	0.024	0.321	0.095	0.158	0.109
275.000 K							
275.160	19.45538	161.569	0.041	0.026	-0.031	-0.255	-0.206
275.160	18.04039	151.090	0.040	0.027	0.010	-0.228	-0.246
275.156	17.02701	143.171	0.039	0.027	0.033	-0.204	-0.262
275.158	16.04189	135.157	0.038	0.028	0.057	-0.169	-0.262
275.156	15.03640	126.678	0.037	0.029	0.075	-0.130	-0.252
275.158	14.03271	117.949	0.036	0.031	0.090	-0.085	-0.230
275.157	13.03333	109.043	0.035	0.032	0.095	-0.041	-0.206
275.156	12.02664	99.915	0.034	0.034	0.093	0.002	-0.180
275.158	11.02115	90.714	0.033	0.037	0.090	0.049	-0.149
275.157	10.01815	81.512	0.032	0.039	0.070	0.077	-0.131
275.157	9.01514	72.368	0.031	0.043	0.047	0.099	-0.115
275.159	8.01265	63.348	0.030	0.048	0.020	0.110	-0.103
275.155	7.00790	54.488	0.029	0.053	-0.006	0.111	-0.095
275.155	6.00636	45.879	0.028	0.061	-0.028	0.105	-0.085
275.155	5.00625	37.537	0.027	0.072	-0.044	0.092	-0.074
275.153	4.00470	29.459	0.026	0.089	-0.045	0.083	-0.055
275.155	2.99059	21.574	0.025	0.117	-0.025	0.084	-0.021
275.155	2.00369	14.179	0.024	0.173	-0.005	0.076	0.005
275.159	1.00341	6.964	0.024	0.340	0.038	0.084	0.048
300.000 K							
300.107	19.87742	141.339	0.039	0.028	0.053	-0.075	-0.062
300.108	19.02634	135.801	0.038	0.028	0.061	-0.065	-0.064
300.109	18.02164	129.075	0.038	0.029	0.070	-0.052	-0.063

300.110	17.02716	122.225	0.037	0.030	0.077	-0.036	-0.057
300.109	16.02478	115.143	0.036	0.031	0.083	-0.019	-0.051
300.109	15.01494	107.849	0.035	0.033	0.087	-0.002	-0.043
300.105	14.01853	100.521	0.034	0.034	0.087	0.016	-0.036
300.107	13.01552	93.038	0.033	0.036	0.086	0.034	-0.029
300.107	12.01365	85.490	0.033	0.038	0.080	0.050	-0.025
300.106	11.01219	77.912	0.032	0.041	0.078	0.071	-0.016
300.104	10.01067	70.322	0.031	0.044	0.067	0.081	-0.015
300.107	9.00988	62.766	0.030	0.048	0.057	0.091	-0.013
300.106	8.00698	55.254	0.029	0.053	0.046	0.097	-0.010
300.107	7.00700	47.853	0.028	0.059	0.038	0.102	-0.004
300.108	6.00601	40.556	0.028	0.068	0.030	0.101	0.001
300.107	5.00426	33.388	0.027	0.080	0.023	0.096	0.006
300.109	4.00415	26.380	0.026	0.098	0.022	0.091	0.016
300.108	3.00315	19.528	0.025	0.129	0.023	0.083	0.025
300.106	2.00269	12.849	0.024	0.189	0.033	0.079	0.040
300.114	1.00270	6.346	0.024	0.372	0.063	0.090	0.070
325.000 K							
325.102	19.92240	124.409	0.037	0.030	-0.038	-0.107	-0.066
325.102	19.03473	119.239	0.036	0.031	-0.037	-0.102	-0.065
325.104	18.02485	113.235	0.036	0.032	-0.034	-0.093	-0.060
325.101	17.02659	107.176	0.035	0.033	-0.033	-0.086	-0.059
325.104	16.02497	100.987	0.034	0.034	-0.030	-0.075	-0.055
325.105	15.01994	94.679	0.034	0.036	-0.028	-0.065	-0.052
325.105	14.01639	88.297	0.033	0.037	-0.027	-0.055	-0.051
325.105	13.01781	81.881	0.032	0.039	-0.027	-0.045	-0.051
325.104	12.01602	75.396	0.031	0.042	-0.027	-0.034	-0.051
325.104	11.01593	68.894	0.031	0.045	-0.024	-0.021	-0.048
325.104	10.01188	62.350	0.030	0.048	-0.029	-0.016	-0.051
325.103	9.00880	55.821	0.029	0.052	-0.031	-0.009	-0.052
325.102	8.00910	49.339	0.029	0.058	-0.034	-0.005	-0.052
325.103	7.00594	42.877	0.028	0.065	-0.035	< 0.001	-0.049
325.102	6.00544	36.488	0.027	0.074	-0.041	-0.002	-0.050
325.104	5.00397	30.164	0.026	0.087	-0.046	-0.006	-0.050
325.104	4.00403	23.933	0.026	0.107	-0.050	-0.012	-0.049
325.105	2.98910	17.703	0.025	0.141	-0.065	-0.031	-0.060
325.104	2.00279	11.755	0.024	0.206	-0.053	-0.026	-0.046
325.110	1.00294	5.831	0.024	0.404	-0.030	-0.013	-0.024
350.000 K							
350.091	19.94877	111.610	0.036	0.032	-0.050	-0.080	-0.013
350.093	19.03368	106.810	0.035	0.033	-0.049	-0.076	-0.012
350.094	18.02103	101.408	0.034	0.034	-0.049	-0.071	-0.011
350.092	17.01185	95.937	0.034	0.035	-0.049	-0.068	-0.012
350.092	16.01717	90.469	0.033	0.037	-0.047	-0.062	-0.012
350.092	15.00954	84.858	0.033	0.038	-0.046	-0.056	-0.014
350.091	14.00976	79.231	0.032	0.040	-0.044	-0.049	-0.016
350.092	13.00725	73.537	0.031	0.043	-0.042	-0.043	-0.019
350.091	12.00753	67.820	0.031	0.045	-0.041	-0.038	-0.022
350.092	11.00601	62.068	0.030	0.048	-0.034	-0.026	-0.019
350.092	10.00977	56.325	0.029	0.052	-0.035	-0.023	-0.023
350.092	9.00567	50.531	0.029	0.057	-0.034	-0.019	-0.025
350.092	8.00758	44.777	0.028	0.063	-0.036	-0.017	-0.029
350.089	7.00517	39.016	0.027	0.070	-0.036	-0.015	-0.029
350.090	6.00418	33.287	0.027	0.080	-0.043	-0.020	-0.036
350.093	5.00418	27.602	0.026	0.094	-0.049	-0.026	-0.041

350.093	4.00362	21.959	0.025	0.116	-0.060	-0.038	-0.051
350.091	2.98613	16.278	0.025	0.152	-0.071	-0.050	-0.060
350.093	2.00296	10.848	0.024	0.222	-0.089	-0.072	-0.079
350.100	1.00296	5.395	0.023	0.435	-0.091	-0.080	-0.084

^(a) Expanded uncertainties ($k = 2$): $U(p > 3)/\text{MPa} = 7.5 \cdot 10^{-5} \cdot \frac{p}{\text{MPa}} + 4 \cdot 10^{-3}$; $U(p < 3)/\text{MPa} = 6.0 \cdot$

$$10^{-5} \cdot \frac{p}{\text{MPa}} + 2 \cdot 10^{-3}; U(T) = 15 \text{ mK}; \frac{U(\rho)}{\text{kg} \cdot \text{m}^{-3}} = 2.5 \cdot 10^4 \frac{\chi_s}{\text{m}^3 \text{kg}^{-1}} + 1.1 \cdot 10^{-4} \cdot \frac{\rho}{\text{kg} \cdot \text{m}^{-3}} + 2.3 \cdot 10^{-2}.$$

Table 6. Statistical analysis of the (p, ρ, T) data sets in relation to the AGA8-DC92 EoS [19], GERG-2008 EoS [20,21], and improved GERG-2008 EoS [52–54] for all the NG mixtures investigated in this study, including literature data for similar mixtures. *AARD* = average absolute value of the relative deviations, *BiasRD* = average relative deviation, *RMSRD* = root mean square relative deviation, *MaxRD* = maximum value of the relative deviations.

Reference ^(a)	x_{H_2}	$N^{(b)}$	Covered ranges		Experimental vs AGA8-DC92 EoS				Experimental vs GERG-2008 EoS				Experimental vs improved GERG-2008 EoS			
			T / K	p / MPa	<i>AARD</i> / %	<i>BiasRD</i> / %	<i>RMSR</i> $D / \%$	<i>MaxR</i> $D / \%$	<i>AARD</i> / %	<i>BiasR</i> $D / \%$	<i>RMSR</i> $D / \%$	<i>MaxR</i> $D / \%$	<i>AARD</i> / %	<i>BiasR</i> $D / \%$	<i>RMSR</i> $D / \%$	<i>MaxR</i> $D / \%$
G 432 (this work)	0	93	260–350	1–20	0.040	−0.033	0.055	0.15	0.043	−0.023	0.063	0.21	0.062	−0.051	0.088	0.28
G 455 (this work)	0.099864	98	260–350	1–20	0.048	−0.016	0.062	0.19	0.11	−0.074	0.16	0.44	0.12	−0.12	0.15	0.38
G 456 (this work)	0.200039	99	260–350	1–20	0.065	0.025	0.088	0.28	0.094	$-\frac{0.003}{9}$	0.12	0.34	0.077	−0.070	0.11	0.30
Lozano-Martín et al., 2024 [32]	0	97	250–350	1–20	0.012	−0.0066	0.018	0.054	0.032	0.032	0.034	0.049	0.019	0.016	0.023	0.051
Lozano-Martín et al., 2024 [32]	0.099928	98	275–350	1–20	0.032	−0.029	0.045	0.19	0.029	−0.021	0.049	0.18	0.047	−0.042	0.070	0.20
Lozano-Martín et al., 2024 [32]	0.199945	99	250–350	1–20	0.033	−0.020	0.039	0.12	0.030	−0.015	0.037	0.11	0.052	−0.043	0.072	0.19

^(a) Only vapor and supercritical phase measurements have been considered.

^(b) Number of experimental points.

Table 7. Derived isothermal compressibility κ_T values for all the reference NG mixtures examined in this study at various temperatures T and pressures p .

$\kappa_T / \text{MPa}^{-1(a)}$					
T / K					
p / MPa	260	275	300	325	350
G 432					
19				0.0484	0.0496
18			0.0494	0.0532	0.0542
17	0.0361	0.0460	0.0556	0.0583	0.0586
16	0.0418	0.0535	0.0623	0.0639	0.0634
15	0.0512	0.0625	0.0698	0.0700	0.0688
14	0.0621	0.0732	0.0780	0.0768	0.0750
13	0.0763	0.0859	0.0871	0.0843	0.0817
12	0.0942	0.0999	0.0970	0.0925	0.0893
11	0.1155	0.1152	0.1078	0.1019	0.0980
10	0.1386	0.1311	0.1196	0.1126	0.1082
9	0.1610	0.1473	0.1329	0.1251	0.1202
8	0.1816	0.1644	0.1484	0.1401	0.1350
7	0.2017	0.1836	0.1674	0.1588	0.1536
6	0.2243	0.2075	0.1919	0.1834	0.1781
5	0.2546	0.2399	0.2254	0.2172	0.2119
4	0.3008	0.2884	0.2753	0.2675	0.2621
3	0.3802	0.3702	0.3587	0.3514	0.3463
2	0.5427	0.5311	0.5206	0.5135	0.5031
G 455 (G 432 + 10 % H ₂)					
19		0.0422	0.0474	0.0492	0.0497
18		0.0474	0.0522	0.0535	0.0537
17	0.0478	0.0532	0.0573	0.0580	0.0578
16	0.0548	0.0599	0.0629	0.0629	0.0623
15	0.0632	0.0675	0.0692	0.0684	0.0674
14	0.0730	0.0761	0.0761	0.0745	0.0730
13	0.0844	0.0856	0.0838	0.0813	0.0794
12	0.0972	0.0961	0.0922	0.0890	0.0867
11	0.1112	0.1076	0.1018	0.0978	0.0951
10	0.1263	0.1202	0.1127	0.1081	0.1050
9	0.1422	0.1342	0.1254	0.1202	0.1169
8	0.1595	0.1502	0.1406	0.1351	0.1315
7	0.1793	0.1695	0.1595	0.1538	0.1500
6	0.2038	0.1942	0.1841	0.1783	0.1744
5	0.2368	0.2278	0.2181	0.2123	0.2083
4	0.2859	0.2776	0.2684	0.2628	0.2587
3	0.3678	0.3607	0.3520	0.3467	0.3429
2	0.5330	0.5243	0.5155	0.5100	0.5014
G 456 (G 432 + 20 % H ₂)					
19	0.0433	0.0462	0.0484	0.0492	0.0492
18	0.0480	0.0505	0.0528	0.0532	0.0532
17	0.0535	0.0559	0.0572	0.0573	0.0570
16	0.0597	0.0615	0.0622	0.0618	0.0613
15	0.0668	0.0679	0.0677	0.0669	0.0660
14	0.0747	0.0749	0.0739	0.0725	0.0714
13	0.0836	0.0828	0.0808	0.0789	0.0776
12	0.0934	0.0915	0.0885	0.0862	0.0846

11	0.1044	0.1014	0.0974	0.0947	0.0928
10	0.1167	0.1126	0.1078	0.1047	0.1025
9	0.1305	0.1256	0.1200	0.1166	0.1142
8	0.1466	0.1411	0.1350	0.1312	0.1287
7	0.1661	0.1602	0.1537	0.1498	0.1471
6	0.1910	0.1850	0.1784	0.1743	0.1715
5	0.2249	0.2190	0.2123	0.2082	0.2053
4	0.2749	0.2693	0.2628	0.2587	0.2557
3	0.3578	0.3530	0.3468	0.3427	0.3399
2	0.5250	0.5181	0.5113	0.5069	0.4998

^(a) Expanded uncertainty ($k = 2$): $U_r(\kappa_T) = 0.7\%$.

References

- [1] Pellegrino S, Lanzini A, Leone P. Greening the gas network – The need for modelling the distributed injection of alternative fuels. *Renew Sustain Energy Rev* 2017;70:266–86. <https://doi.org/10.1016/j.rser.2016.11.243>.
- [2] Nemmour A, Inayat A, Janajreh I, Ghenai C. Green hydrogen-based E-fuels (E-methane, E-methanol, E-ammonia) to support clean energy transition: A literature review. *Int J Hydrogen Energy* 2023;48:29011–33. <https://doi.org/10.1016/j.ijhydene.2023.03.240>.
- [3] Ruiz Diaz DF, Zhao J, Ming Quamg Pham J, Ramirez C, Qin H, Jimenez AJ, Pulianda AM, Chaudhary C, McDonell V, Li GP. Mathematical modeling for hydrogen blending in NG pipelines moving towards industrial decarbonization: Economic feasibility and CO₂ reduction analysis. *Int J Hydrogen Energy* 2024;88:1422–35. <https://doi.org/10.1016/j.ijhydene.2024.09.083>.
- [4] Topolski K, Reznicek EP, Erdener BC, San Marchi CW, Ronevich JA, Fring L, Simmons K, Guerra Fernandez OJ, Hodge B-M, Chung M. Hydrogen Blending into NG Pipeline Infrastructure: Review of the State of Technology. Natl Renew Energy Lab NREL/TP5400-81704, Golden CO, 2022.
- [5] Bard J, Gerhardt N, Selzam P, Beil M, Wiemer M BM. The limitations of hydrogen blending in the European gas grid. Fraunhofer Inst Energy Econ Energy Syst Technol (IEE), Kassel 2022.
- [6] Quarton CJ, Samsatli S. Power-to-gas for injection into the gas grid: What can we learn from real-life projects, economic assessments and systems modelling? *Renew Sustain Energy Rev* 2018;98:302–16. <https://doi.org/10.1016/j.rser.2018.09.007>.
- [7] Erdener BC, Sergi B, Guerra OJ, Lazaro Chueca A, Pambour K, Brancucci C, Hodge B-M. A review of technical and regulatory limits for hydrogen blending in NG pipelines. *Int J Hydrogen Energy* 2023;48:5595–617. <https://doi.org/10.1016/j.ijhydene.2022.10.254>.
- [8] Chen Y, Niu J, Liu W, Long L, Huang T, Sun Y, Wan Z, Yu B. Experimental analysis and modeling on the blending limit of domestic burner with porous media for hydrogen enriched NG. *Int J Hydrogen Energy* 2024;88:1321–31. <https://doi.org/10.1016/j.ijhydene.2024.09.263>.

- [9] Lo Basso G, Pastore LM, Sgaramella A, Mojtahed A, de Santoli L. Recent progresses in H₂NG blends use downstream Power-to-Gas policies application: An overview over the last decade. *Int J Hydrogen Energy* 2024; 51:424-53. <https://doi.org/10.1016/j.ijhydene.2023.06.141>.
- [10] Makaryan IA, Sedov I V., Salgansky EA, Arutyunov A V., Arutyunov VS. A Comprehensive Review on the Prospects of Using Hydrogen–Methane Blends: Challenges and Opportunities. *Energies* 2022;15:2265. <https://doi.org/10.3390/en15062265>.
- [11] Rodrigues NS, McDonald CT, Busari OO, Satija A, Lucht RP. Transverse injection of rich, premixed, NG-air and NG-hydrogen-air reacting jets into high-speed vitiated crossflow at engine-relevant conditions. *Int J Hydrogen Energy* 2021;46:35718–38. <https://doi.org/10.1016/j.ijhydene.2021.08.108>.
- [12] Fichtner J, Gegner A, Ninow J, Kapischke J. Hydrogen enriched NG as fuel for CHP units. *Int J Hydrogen Energy* 2023;48:35280–90. <https://doi.org/10.1016/j.ijhydene.2023.05.263>.
- [13] Schwarz S, Daurer G, Gaber C, Demuth M, Prieler R, Hochenauer C. Experimental investigation of the combustion characteristics in oxy-fuel combustion of hydrogen-enriched NG on a semi-industrial scale. *Int J Hydrogen Energy* 2024;49:323-37. <https://doi.org/10.1016/j.ijhydene.2023.07.268>.
- [14] Jia G, Lei M, Li M, Xu W, Li R, Lu Y, Cai M. Hydrogen embrittlement in hydrogen-blended NG transportation systems: A review. *Int J Hydrogen Energy* 2023;48:32137–57. <https://doi.org/10.1016/j.ijhydene.2023.04.266>.
- [15] Wu X, Zhang H, Yang M, Jia W, Qiu Y, Lan L. From the perspective of new technology of blending hydrogen into NG pipelines transmission: Mechanism, experimental study, and suggestions for further work of hydrogen embrittlement in high-strength pipeline steels. *Int J Hydrogen Energy* 2022;47:8071–90. <https://doi.org/10.1016/j.ijhydene.2021.12.108>.
- [16] Wang H, Tong Z, Zhou G, Zhang C, Zhou H, Wang Y, Zheng W. Research and demonstration on hydrogen compatibility of pipelines: a review of current status and challenges. *Int J Hydrogen Energy* 2022;47:28585–604. <https://doi.org/10.1016/j.ijhydene.2022.06.158>.
- [17] Kontogeorgis GM, Dohrn R, Economou IG, de Hemptinne J-C, ten Kate A, Kuitunen S, Mooijer M, Fele Žilnik L, Vesovic V. Industrial Requirements for Thermodynamic and Transport Properties:

2020. *Ind Eng Chem Res* 2021;60:4987–5013. <https://doi.org/10.1021/acs.iecr.0c05356>.
- [18] Hendriks E, Kontogeorgis GM, Dohrn R, De Hemptinne JC, Economou IG, Žilnik LF, Fele Žilnik L, Vesovic V. Industrial requirements for thermodynamics and transport properties. *Ind Eng Chem Res* 2010;49:11131–41. <https://doi.org/10.1021/ie101231b>.
- [19] Transmission Measurement Committee. AGA Report No. 8 Part 1 Thermodynamic Properties of NG and Related Gases DETAIL and GROSS Equations of State. Washington DC: 2017.
- [20] Kunz O, Klimeck R, Wagner W, Jaeschke M. The GERG-2004 Wide-Range Equation of State for NGes and Other Mixtures. *Fortschritt-Berichte VDI*, Düsseldorf: 2007.
- [21] Kunz O, Wagner W. The GERG-2008 Wide-Range Equation of State for NGes and Other Mixtures: An Expansion of GERG-2004. *J Chem Eng Data* 2012;57:3032–91. <https://doi.org/10.1021/je300655b>.
- [22] Lozano-Martín D, Moreau A, Chamorro CR. Thermophysical properties of hydrogen mixtures relevant for the development of the hydrogen economy: Review of available experimental data and thermodynamic models. *Renew Energy* 2022;198:1398–429. <https://doi.org/10.1016/j.renene.2022.08.096>.
- [23] Leusmann Y, Klink S, Vega-Maza D, Richter M. Dew points for hydrogen-rich (hydrogen + propane) and (hydrogen + n-butane) mixtures determined with a microwave re-entrant cavity resonator. *Fuel* 2024;377:132583. <https://doi.org/10.1016/j.fuel.2024.132583>.
- [24] Owuna FJ, Chapoy A, Ahmadi P, Burgass R. Experimental (ρ, P, T) data of $H_2 + CH_4$ mixtures at temperatures from 278 to 398 K and pressures up to 56 MPa. *Int J Hydrogen Energy* 2024;68:979–97. <https://doi.org/10.1016/j.ijhydene.2024.04.244>.
- [25] Lozano-Martín D, Khanipour P, Kipphardt H, Tuma D, Chamorro CR. Thermodynamic characterization of the ($H_2 + C_3H_8$) system significant for the hydrogen economy: Experimental (p, ρ, T) determination and equation-of-state modelling. *Int J Hydrogen Energy* 2023;48:8645–67. <https://doi.org/10.1016/j.ijhydene.2022.11.170>.
- [26] Lozano-Martín D, Martín MC, Chamorro CR, Tuma D, Segovia JJ. Speed of sound for three binary ($CH_4 + H_2$) mixtures from $p = (0.5 \text{ up to } 20) \text{ MPa}$ at $T = (273.16 \text{ to } 375) \text{ K}$. *Int J Hydrogen Energy* 2020;45:4765–83. <https://doi.org/10.1016/j.ijhydene.2019.12.012>.

- [27] Hernández-Gómez R, Tuma D, Pérez E, Chamorro CR. Accurate Experimental (p , ρ , and T) Data for the Introduction of Hydrogen into the NG Grid (II): Thermodynamic Characterization of the Methane–Hydrogen Binary System from 240 to 350 K and Pressures up to 20 MPa. *J Chem Eng Data* 2018;63:1613–30. <https://doi.org/10.1021/acs.jced.7b01125>.
- [28] Hernández-Gómez R, Tuma D, Gómez-Hernández A, Chamorro CR. Accurate Experimental (p , ρ , T) Data for the Introduction of Hydrogen into the NG Grid: Thermodynamic Characterization of the Nitrogen–Hydrogen Binary System from 240 to 350 K and Pressures up to 20 MPa. *J Chem Eng Data* 2017;62:4310–26. <https://doi.org/10.1021/acs.jced.7b00694>.
- [29] Deymi-Dashtebayaz M, Ebrahimi-Moghadam A, Pishbin SI, Pourramezan M. Investigating the effect of hydrogen injection on NG thermo-physical properties with various compositions. *Energy* 2019;167:235–45. <https://doi.org/10.1016/j.energy.2018.10.186>.
- [30] Al Ghafri SZS, Jiao F, Hughes TJ, Arami-Niya A, Yang X, Siahvashi A, Karimi A, May EF. NG density measurements and the impact of accuracy on process design. *Fuel* 2021;304:121395. <https://doi.org/10.1016/j.fuel.2021.121395>.
- [31] Hernández-Gómez R, Tuma D, Lozano-Martín D, Chamorro CR. Accurate experimental (p , ρ , T) data of NG mixtures for the assessment of reference equations of state when dealing with hydrogen-enriched NG. *Int J Hydrogen Energy* 2018;43:21983–98. <https://doi.org/10.1016/j.ijhydene.2018.10.027>.
- [32] Lozano-Martín D, Pazoki F, Kipphardt H, Khanipour P, Tuma D, Horrillo A, Chamorro CR. Thermodynamic (p , ρ , T) characterization of a reference high-calorific NG mixture when hydrogen is added up to 20 % (mol/mol). *Int J Hydrogen Energy* 2024;70:118–35. <https://doi.org/10.1016/j.ijhydene.2024.05.028>.
- [33] International Organization for Standardization. ISO 6142-1 Gas analysis — Preparation of calibration gas mixtures — Part 1: Gravimetric method for Class I mixtures. Genève: 2014.
- [34] International Organization for Standardization, International Organization for Standardization. ISO 12963. ISO 12963. Gas analysis – Comparison methods for the determination of the composition of gas mixtures based on one- and two-point calibration. Genève: 2017.
- [35] Joint Comitee for Guides in Metrology, JCGM100:2008, GUM1995. Evaluation of measurement

- data — Guide to the expression of uncertainty in measurement. JCGM 1002008 GUM 1995 with Minor Correct 2008.
- [36] Lemmon, E.W., Bell, I.H., Huber, M.L., McLinden MO. NIST Standard Reference Database 23: Reference Fluid Thermodynamic and Transport Properties-REFPROP, Version 10.0. Natl Inst Stand Technol Stand Ref Data Progr 2018.
- [37] Huber ML, Lemmon EW, Bell IH, McLinden MO. The NIST REFPROP Database for Highly Accurate Properties of Industrially Important Fluids *Ind Eng Chem Res* 2022;61:15449–72. <https://doi.org/10.1021/acs.iecr.2c01427>.
- [38] Kleinrahm R, Wagner W. Measurement and correlation of the equilibrium liquid and vapour densities and the vapour pressure along the coexistence curve of methane. *J Chem Thermodyn* 1986;18:739–60. [https://doi.org/10.1016/0021-9614\(86\)90108-4](https://doi.org/10.1016/0021-9614(86)90108-4).
- [39] Lösch HW, Kleinrahm R, Wagner W. Neue Magnetschwebewaagen für gravimetrische Messungen in der Verfahrenstechnik. *Chem Ing Tech* 1994;66:1055–8. <https://doi.org/10.1002/cite.330660808>.
- [40] Yang X, Kleinrahm R, McLinden MO, Richter M. The Magnetic Suspension Balance: 40 Years of Advancing Densimetry and Sorption Science. *Int J Thermophys* 2023;44:169. <https://doi.org/10.1007/s10765-023-03269-0>.
- [41] Wagner W, Kleinrahm R. Densimeters for very accurate density measurements of fluids over large ranges of temperature, pressure, and density. *Metrologia* 2004;41:S24–39. <https://doi.org/10.1088/0026-1394/41/2/S03>.
- [42] Wagner W, Brachthäuser K, Kleinrahm R, Lösch HW. A new, accurate single-sinker densitometer for temperatures from 233 to 523 K at pressures up to 30 MPa. *Int J Thermophys* 1995;16:399–411. <https://doi.org/10.1007/BF01441906>.
- [43] Klimeck J, Kleinrahm R, Wagner W. An accurate single-sinker densimeter and measurements of the (p, ρ, T) relation of argon and nitrogen in the temperature range from (235 to 520) K at pressures up to 30 MPa. *J Chem Thermodyn* 1998;30:1571–88.
- [44] McLinden MO, Kleinrahm R, Wagner W. Force Transmission Errors in Magnetic Suspension Densimeters. *Int J Thermophys* 2007;28:429–48. <https://doi.org/10.1007/s10765-007-0176-0>.
- [45] Lozano-Martín D, Mondéjar ME, Segovia JJ, Chamorro CR. Determination of the force

- transmission error in a single-sinker magnetic suspension densimeter due to the fluid-specific effect and its correction for use with gas mixtures containing oxygen. *Measurement* 2020;151:107176. <https://doi.org/10.1016/j.measurement.2019.107176>.
- [46] Kleinrahm R, Yang X, McLinden MO, Richter M. Analysis of the systematic force-transmission error of the magnetic-suspension coupling in single-sinker densimeters and commercial gravimetric sorption analyzers. *Adsorption* 2019;25:717–35. <https://doi.org/10.1007/s10450-019-00071-z>
- [47] Lozano-Martín D, Akubue GU, Moreau A, Tuma D, Chamorro CR. Accurate experimental (p, ρ, T) data of the ($\text{CO}_2 + \text{O}_2$) binary system for the development of models for CCS processes. *J Chem Thermodyn* 2020;150:106210. <https://doi.org/10.1016/j.jct.2020.106210>.
- [48] Lozano-Martín D, Vega-Maza D, Martín MC, Tuma D, Chamorro CR. Thermodynamic characterization of the ($\text{CO}_2 + \text{O}_2$) binary system for the development of models for CCS processes: Accurate experimental (p, ρ, T) data and virial coefficients. *J Supercrit Fluids* 2021;169:105074. <https://doi.org/10.1016/j.supflu.2020.105074>.
- [49] Chamorro CR, Segovia JJ, Martín MC, Villamañán MA, Estela-Uribe JF, Trusler JPM. Measurement of the (pressure, density, temperature) relation of two (methane+nitrogen) gas mixtures at temperatures between 240 and 400 K and pressures up to 20 MPa using an accurate single-sinker densimeter. *J Chem Thermodyn* 2006;38:916–22. <https://doi.org/10.1016/j.jct.2005.10.004>.
- [50] Mondéjar ME, Segovia JJ, Chamorro CR. Improvement of the measurement uncertainty of a high accuracy single sinker densimeter via setup modifications based on a state point uncertainty analysis. *Measurement* 2011;44:1768–80. <https://doi.org/10.1016/j.measurement.2011.07.012>.
- [51] Joint Committee for Guides in Metrology (JCGM). Evaluation of measurement data: Guide to the expression of uncertainty in measurement 2008:120.
- [52] International Organization for Standardization. ISO 20765-2 NG — Calculation of thermodynamic properties — Part 2: Single-phase properties (gas, liquid, and dense fluid) for extended ranges of application. Genève: 2013.
- [53] Thol M, Richter M, May EF, Lemmon EW, Span R. EOS-LNG: A Fundamental Equation of State

- for the Calculation of Thermodynamic Properties of Liquefied NGe. *J Phys Chem Ref Data* 2019;48:033102. <https://doi.org/10.1063/1.5093800>.
- [54] Beckmüller R, Thol M, Bell IH, Lemmon EW, Span R. New Equations of State for Binary Hydrogen Mixtures Containing Methane, Nitrogen, Carbon Monoxide, and Carbon Dioxide. *J Phys Chem Ref Data* 2021;50:013102. <https://doi.org/10.1063/5.0040533>.
- [55] International Organization for Standardization. ISO 20765-1 NG — Calculation of thermodynamic properties — Part 1: Gas phase properties for transmission and distribution applications. Genève: 2005.
- [56] Lentner R, Richter M, Kleinrahm R, Span R. Density measurements of liquefied NG (LNG) over the temperature range from (105 to 135) K at pressures up to 8.9 MPa. *J Chem Thermodyn* 2017;112:68–76. <https://doi.org/10.1016/j.jct.2017.04.002>.
- [57] Lentner R, Eckmann P, Kleinrahm R, Span R, Richter M. Density measurements of seven methane-rich binary mixtures over the temperature range from (100 to 180) K at pressures up to 9.7 MPa. *J Chem Thermodyn* 2020;142:106002. <https://doi.org/10.1016/j.jct.2019.106002>.
- [58] Richter M, Kleinrahm R. Influence of adsorption and desorption on accurate density measurements of gas mixtures. *J Chem Thermodyn* 2014;74:58–66. <https://doi.org/10.1016/j.jct.2014.03.020>.